HHS Public Access

Author manuscript

Cell Rep. Author manuscript; available in PMC 2021 September 07.

Published in final edited form as:

Cell Rep. 2021 January 12; 34(2): 108603. doi:10.1016/j.celrep.2020.108603.

NOTCH Signaling Controls Ciliary Body Morphogenesis and Secretion by Directly Regulating Nectin Protein Expression

Ji Pang[1,2], **Liang Le**[1,#], **Yi Zhou**[1,3,#], **Renjun Tu**[1], **Qiang Hou**[1,4], **Dai Tsuchiya**[1], **Nancy Thomas**[1], **Yongfu Wang**[1], **Zulin Yu**[1], **Richard Alexander**[1], **Marina Thexton**[1], **Brandy Lewis**[1], **Timothy Corbin**[1], **Michael Durnin**[1], **Hua Li**[1], **Ruth Ashery-Padan**[5], **Deyue Yan**[2], **Ting Xie**[1,3,*]

[1]Stowers Institute for Medical Research, 1000 East 50th Street, Kansas City, MO 64110, USA

[2]School of Chemistry and Chemical Engineering, State Key Laboratory of Metal Matrix Composites, Shanghai Jiao Tong University, 800 Dongchuan Road, Shanghai 200240, China

[3]Department of Anatomy and Cell Biology, University of Kansas School of Medicine, 3901 Rainbow Blvd, Kansas City, KS 66160, USA

[4]State Key Laboratory and Key Laboratory of Vision Science, School of Ophthalmology and Optometry, Eye Hospital, Wenzhou Medical University, Wenzhou, Zhejiang, China

[5]Department of Human Molecular Genetics and Biochemistry, Sackler Faculty of Medicine, Tel Aviv University, Tel Aviv, Israel

Summary

Anterior segment dysgenesis is often associated with cornea diseases, cataracts and glaucoma. In the anterior segment, the ciliary body (CB) containing inner and outer ciliary epithelia (ICE and OCE) secretes aqueous humor that maintains intraocular pressure (IOP). However, CB development and function remain poorly understood. Here, this study shows that NOTCH signaling in the CB maintains the vitreous, IOP and eye structures by regulating CB morphogenesis, aqueous humor and vitreous protein secretion. *Notch2* and *Notch3* function via RBPJ in the CB to control ICE-OCE adhesion, CB morphogenesis, aqueous humor and protein secretion, thus maintaining IOP and eye structures. Mechanistically, NOTCH signaling controls transcriptionally Nectin1 expression in the OCE to promote cell adhesion for driving CB morphogenesis and directly stabilize Cx43 for controlling aqueous humor secretion. Finally, NOTCH signaling directly controls vitreous protein secretion in the ICE. Therefore, this study provides important insight into CB functions and involvement in eye diseases.

*Correspondence and Lead Contact: Dr. Ting Xie tgx@stowers.org.

#Those contributed equally

Author Contributions

J.P. and T.X., conceived the study, analyzed data and wrote the manuscript; J.P., L.L., Y.Z., R.T., Q.H., D.T., N.T., Y.W., Z.Y., R.A., M.T., B.L., T.C., M.D., H.L., performed the experiments; R.A-P., provided the *Tyrp2-Cre* mouse strain; D.Y. and T.X., supervision.

Declaration of Interests

The authors declare no competing interests.

Introduction

The congenital developmental disorders affecting the anterior segment of the eye are collectively known as anterior segment dysgenesis (ASD), which is associated with 50% risk for glaucoma (Reis and Semina, 2011). As a part of the anterior segment, the ciliary body (CB) consists of three major components: non-pigmented inner ciliary epithelium (ICE), pigmented outer ciliary epithelium (OCE), and the underlying stroma and blood vessels (Beebe, 1986; Gage et al., 2005). It has two important biological functions: lens accommodation and production of aqueous and vitreous humor. The aqueous humor nourishes avascular anterior structures and generates the intraocular pressure (IOP), whose elevation is often a risk factor for glaucoma (Stamer and Acott, 2012; Zhang et al., 2012). In addition, zonule fibers extended from the CB controls the lens accommodation, which defects can lead to myopia or nearsightedness (Curtin, 1979; Morgan et al., 2012). Finally, the CB also secretes extracellular matrix (ECM) proteins, growth factors and other proteins into the anterior chamber and the vitreous body to nourish various eye structures. In spite of the importance of the CB in the mammalian eye, the mechanisms underlying CB development and secretion remain poorly understood.

The CB develops from the ciliary marginal zone (CMZ) at the rim of the optic cup. Genetic studies have identified several important pathways and regulators that control CB specification. FGF signaling controls the patterning of the presumptive CB region, while Wnt signaling and miRNA biogenesis key enzyme Dicer1 are required for CB specification (Cho and Cepko, 2006; Dias da Silva et al., 2007; Kubo et al., 2003; Liu et al., 2007;Davis et al., 2011). Following the specification, ciliary folds form during the first week after birth (Beebe, 1986; Zhou et al., 2013). BMP signaling has been shown to be crucial for this process: BMP4 haploinsufficiency or ectopic expression of BMP inhibitor Noggin severely impair CB morphogenesis (Chang et al., 2001; Zhao et al., 2002). Nectin1 and 3 are expressed in OCE and ICE, respectively, to maintain ICE-OCE adhesion for promoting CB morphogenesis (Inagaki et al., 2005). In addition, TSC1-regulated mTORC1 activities are important for promoting cell proliferation and CB morphogenesis (Hagglund et al., 2017). We have recently shown that JAG1 and NOTCH2 regulate CB fold formation by maintaining cell proliferation and BMP signaling in the OCE (Zhou et al., 2013). Inactivating the NOTCH downstream transcriptional factor RBPJ in the CB also consistently leads to the complete CB loss and eye degeneration, whereas constitutive Notch signaling increases IOP due to CB hyperplasia (Sarode et al., 2014). However, it remains unclear why the *Rbpj* mutant CB causes much severe eye phenotypes than the *Notch2* mutant CB. This study has shown that NOTCH3 function redundantly with NOTCH2 in the CB to drive CB morphogenesis by regulating the expression of adhesion molecule Nectin1.

The CB secrets liquid aqueous humor for providing nutritive support for the cornea, the lens, the trabecular meshwork and the retina, and also for maintaining IOP (Coca-Prados and Escribano, 2007; Delamere, 2005). The mechanosensitive cation-permeable channel protein TRPV4 is required in the CB for controlling aqueous humor secretion, suggesting that the mechanic force generating by IOP fluctuation might modulate aqueous humor secretion (Jo et al., 2016). Consistently, mechanosensitive gap junctional protein Connexin43 (Cx43) is required in the CB to control aqueous humor secretion and maintain IOP (Calera et al.,

2006; Calera et al., 2009). Human and mouse CBs can secrete various proteins into the vitreous, including Opticin (Optc) and collagens (Bishop et al., 2002; Skeie et al., 2015). Interestingly, 35 glaucoma-related genes are also expressed in the human CB (Janssen et al., 2012). Although Cx43 and Nectin proteins have been shown to be required for maintaining the vitreous (Calera et al., 2006; Inagaki et al., 2005), it remains unclear how they are regulated in the CB at the molecular level. In this study, we have shown that canonical NOTCH signaling controls the expression of Nectin1 in the OCE for promoting CB morphogenesis and aqueous humor secretion, and also directly controls the expression of vitreous proteins in the ICE. Therefore, our findings have provided important insight into how NOTCH signaling controls CB morphogenesis and secretion, which also implicates the dysfunctional CB in various eye diseases.

Results

NOTCH2 and NOTCH3 contribute to NOTCH-RBPJ signaling for controlling ICE-OCE adhesion and CB fold formation

To understand why inactivating *Rbpj* but not *Notch2* in the RPE causes eye degeneration (Sarode et al., 2014; Zhou et al., 2013), we reexamined the mutant phenotypes of the conditional *Rbpj* and *Notch2* knockout eyes using *Tyrp2-Cre*, which can efficiently delete a floxed gene throughout the iris, the CB and the RPE (Davis et al., 2009)(Fig. S1). Consistent with our previous finding (Zhou et al., 2013), *Tyrp2-Cre; Notch2*$^{fx/fx}$ (thereafter referred to as the *Notch2* mutant) eyes completely lack any CB fold formation but still maintain ICE-OCE adhesion in the CB compared to control P7 eyes containing 3 to 4 ciliary folds in the CB (Fig. S1; Fig. 1A). *Tyrp2-Cre; Rbpj*$^{fx/fx}$ (the *Rbpj* mutant) eyes show no CB morphogenesis, a shortened CB region and iris dysgenesis as previously reported (Sarode et al., 2014) (Fig. 1B). The shortened CB is likely caused by the decreased cell proliferation in both the ICE and the OCE of the *Rbpj* mutant CB (Fig. S2). Surprisingly, the *Rbpj* mutant eyes frequently exhibit the self-folded ICE stem in the CB and the separated ICE folded on the top of the retina, which result from the separation of the ICE and the OCE in the developing CB, suggesting that RBPJ is required in the developing CB for maintaining ICE-OCE adhesion (Fig. 1B' and 1B"). Additionally, the *Rbpj* mutant eyes often carry neural rosettes in the periphery of the retina, which are likely caused by defective retinal cell adhesion (Fig. 1B"; Fig. S1). Quantitatively, 68% of the *Rbpj* mutant eyes exhibit defective ICE-OCE adhesion in the developing CB (Fig. 1C). Since *Jag1* and *Notch2* mutant CBs manifest weaker phenotypes than *Rbpj* mutant ones (Zhou et al., 2013), our results suggest that additional NOTCH receptors and ligands might be involved in controlling CB development through RBPJ.

Our previous microarray results indicate that additional NOTCH ligand and receptor, *Delta-like 1* (*Dll1*) and *Notch3*, are expressed in the developing CB in addition to *Jag1* and *Notch2* (Zhou et al., 2013). Then, we used mRNA fluorescent *in situ* hybridization (FISH) to confirm their expression and determine their detailed expression patterns in the developing CB. In the P7 CB, *Jag1*, *Dll1* and *Rbpj* are expressed in both the ICE and the OCE with higher levels in the ICE, whereas *Notch2* and *Notch3* are also expressed in both the ICE and OCE but with higher levels in the OCE (Fig. S3). Interestingly, the *Notch3*

deletion mutant CB is morphologically normal compared to the control (Fig. 1C and 1D). However, the *Notch2/3* double mutant CB exhibits no fold formation with 18.1% having defective ICE-OCE epithelial adhesion (Fig. 1C and 1E). The *Notch2/3* double mutant and *Rbpj* mutant CBs share similar ICE-OCE adhesion defects, but not *Notch2* or *Notch3* mutant CBs, suggesting the functional redundancy between NOTCH2 and NOTCH3 in the regulation of CB development (Fig. 1C).

To further delineate NOTCH2 and NOTCH3 redundancy in the CB, we used mRNA FISH to quantify the expression levels of two known NOTCH target genes, *Hes1* and *Hey1*, in the control, *Notch2*, *Notch3*, *Notch2/3* and *Rbpj* mutant P7 CBs (Andersson et al., 2011; Mumm and Kopan, 2000). In the control CB, *Hes1* is expressed in both the ICE and the OCE but higher in the ICE, whereas *Hey1* is primarily expressed in the OCE, indicating that NOTCH signaling is active in both the ICE and the OCE but have distinct transcriptional responses (Fig. 1F–G). Based on *Hes1* and *Hey1* expression, both *Notch2* and *Notch3* mutant CBs exhibit significant NOTCH signaling defects in both the ICE and the OCE, but the *Notch2* mutant has more severe NOTCH signaling defects in the OCE than the *Notch3* mutant, which is consistent with their different requirements for CB development (Fig. 1H–J"). The *Notch2/3* double and *Rbpj* mutant CBs have similar NOTCH signaling defects in both the ICE and the OCE based on *Hes1* and *Hey1* expression but they show significantly lower NOTCH signaling in the OCE than the *Notch2* and *Notch3* mutant CBs based on *Hes1* expression, supporting the redundant function of NOTCH2 and NOTCH3 in NOTCH signaling (Fig. 1H–L"). It is worth noting that NOTCH2 and NOTCH3 contribute similarly to NOTCH signaling in the ICE based on *Hes1* expression (Fig. 1I). Based on the expression of the known CB markers, *Msx1* and *Otx1*, the *Notch2/3* double and *Rbpj* mutant CBs still maintain their normal cell identity, suggesting that their CB developmental defects are not caused by the changed cell identities (Fig. S4). These results indicate that NOTCH2 and NOTCH3 collectively contribute to NOTCH-RBPJ signaling activities in both the ICE and the OCE, and function redundantly at least in the OCE, to regulate CB development. Since the *Notch2/3* double mutant CBs show less severe phenotypes than the *Rbpj* mutant ones though exhibiting comparable defects in NOTCH signaling, RBPJ could have a NOTCH signaling-independent function(s) in the regulation of CB development.

NOTCH signaling controls *Nectin1* and *Nectin3* expression in the OCE for promoting ICE-OCE adhesion and CB morphogenesis

Adhesion molecule Nectin1 is primarily expressed in the OCE, whereas its closely related protein Nectin3 is expressed in the ICE and the OCE: Nectin1 and Nectin3 accumulate at the apical side for mediating ICE-OCE epithelial adhesion, thus promoting CB morphogenesis and the formation of the vitreous body (Inagaki et al., 2005). Since the *Notch2/3* and *Rbpj* mutant CBs share similar phenotypes with the previously reported *Nectin1* and *Nectin3* mutant CBs, we then used mRNA FISH to examine the expression of *Nectin1* and *Nectin3* mRNAs in control, *Notch2/3* and *Rbpj* mutant CBs. Our results have confirmed that *Nectin1* mRNA is primarily expressed in the OCE of the control P7 CB, whereas *Nectin3* mRNA is present in both the ICE and OCE with higher levels in the ICE (Fig. 2A–A" and 2D). Interestingly, *Nectin1* and *Nectin3* mRNAs are significantly decreased in the OCE of the *Notch2/3* and *Rbpj* mutant CBs compared to the control CB, but *Nectin1* is more severely

affected than *Nectin3* (Fig. 2B–2D). *Nectin3* mRNA levels remain largely unchanged in the ICE between the control and the mutants (Fig. 2B–2D). These results indicate that NOTCH signaling regulates the expression of *Nectin1* and *Nectin3* in the OCE of the developing CB.

Consistent with the previous report (Inagaki et al., 2005), Nectin1 protein is enriched on both the apical and the lateral sides of the OCE, whereas Nectin3 protein is enriched on the apical side of the ICE to presumably engage with Nectin1 on the apical side of the OCE to mediate ICE-OCE epithelial adhesion (Fig. 2E–E' and S5A–A'). Consistent with its mRNA expression, Nectin3 protein is also present in the OCE at low levels (Fig. S5A–A'). In addition, Nectin1 also highly accumulates on the apical side of the neural retina and the RPE, and Nectin3 is enriched on the apical side of the retina, to possibly mediate the retina-RPE adhesion. Compared to the control CB, the *Rbpj* mutant CB drastically decreases apical and lateral Nectin1 protein accumulation in the OCE and show the apical-to-lateral relocation of Nectin3 protein in the ICE, which could be caused by the loss of the apical accumulation of Nectin1 protein in the OCE (Fig. 2F–F'; S5B–B'). These results indicate that NOTCH signaling regulates the expression of *Nectin* genes in the OCE of the developing CB to maintain ICE-OCE epithelial adhesion.

RBPJ has been established to bind the well-defined consensus site, TGGGAA, to regulate the transcription of downstream target genes, include *Hes1* and *Hey1* (Kulic et al., 2015; Wang et al., 2011). Interestingly, our bioinformatics analysis has identified 7 consensus RBPJ binding sites within the promoter, the first exon and the first large intron of the *Nectin1* gene (Fig. 2G). Our chromatin immunoprecipitation (ChIP)-qPCR results on the isolated CBs have confirmed that RBPJ indeed occupies these sites in the *Nectin1* gene *in vivo*. These results suggest that RBPJ directly regulates *Nectin1* transcription.

Nectin 1 is a major NOTCH target in the OCE for promoting ICE-OCE adhesion and CB morphogenesis

Since *Nectin1* is more severely downregulated in the *Rbpj* mutant CB than *Nectin3*, we then tested if forced *Nectin1* expression in the *Rbpj* mutant CB could rescue its ICE-OCE adhesion and morphogenesis defects by generating a *CAG-LoxP-STOP-LoxP-Nectin1* transgene. Our mRNA FISH results show that CB/RPE-specific overexpression of *Nectin1* (*Nectin1*^{OE}) in the *Rbpj* mutant CB can significantly restore *Nectin1* mRNA expression levels in the OCE, but does not achieve its normal expression levels (Fig. S6). Indeed, our immunofluorescent staining and Western blotting results indicate that *Nectin1*^{OE} can significantly restore Nectin1 protein expression in the *Rbpj* mutant CB and achieve the proper lateral localization of Nectin1 protein in the mutant OCE (Fig. 3A–E). Interestingly, *Nectin1*^{OE} in the *Rbpj* mutant CB can prevent the ICE-OCE separation and partially restore CB morphogenesis (Fig. 3F–I). In addition, it can also partially rescue the rosette formation phenotype in the periphery retina of the *Rbpj* mutant, suggesting that NOTCH signaling also controls the expression of *Necin1* to mediate retinal cell adhesion (Fig. 3F–H' and 3J). Since Nectin1 overexpression can partially rescue the ICE-OCE adhesion and CB morphogenetic defects, these results indicate that Nectin1 is a major NOTCH target in the OCE to control ICE-OCE adhesion, CB morphogenesis, and retinal cell adhesion, and further suggest that other targets, such as Nectin3, are also important for CB development.

NOTCH-RBPJ signaling in the CB maintains the vitreous body and IOP in adult eyes

In the previous report (Sarode et al., 2014), inactivating *Rbpj* function in the CB/RPE results in the loss of the vitreous body in adult eyes, but it remains unclear when such phenotype begins and what causes it. To the end, we re-examined the vitreous body and IOP in the control, *Notch2*, *Notch3*, *Notch2/3* and *Rbpj* mutant eyes. Compared to the P7 control eyes, *Notch2* and *Notch3* mutant eyes exhibit a slightly small vitreous body, and *Notch2/3* and *Rbpj* mutant eyes show a much smaller vitreous body (Fig. 4A–E). Quantitatively, *Notch2/3* and *Rbpj* mutants significantly decrease the depth of the vitreous body compared to *Notch2* and *Notch3* mutants (Fig. 4F). Such the vitreous body defects persist in *Notch2/3* and *Rbpj* mutant adult eyes (Fig. 4G and 4H). Although the P7 *Notch2/3* and *Rbpj* mutant eyes do not show any sign of degeneration, interestingly, 82.6% (n=23) of the *Rbpj* mutant adult eyes and 23.5% (n=17) of *Notch2/3* mutant eyes completely degenerate by the age of 4 moths, losing all the eye structures (Fig 4I and 4J). Surprisingly, both *Notch2* and *Notch3* mutant adult eyes show a lower IOP compared than the control (Fig. 4K). In addition, *Rbpj* and *Notch2/3* mutant adult eyes have significantly lower IOP than *Notch2* and *Notch3* mutant adult eyes (Fig. 4K). These results indicate that NOTCH2 and NOTCH3 function redundantly to maximize NOTCH-RBPJ signaling in the CB, thereby maintaining the vitreous body and IOP. However, we could not completely rule out the possibility that NOTCH3 indirectly contributes to the ocular phenotypes through its function outside the eye since *Notch3* is deleted in all the tissues.

NOTCH signaling maintains the expression of gap junction protein Cx43 in the OCE

Since *Notch2/3* and *Rbpj* mutant eyes show obvious defects in maintaining IOP and eye structures, we then investigated the potential role of NOTCH signaling in the regulation of CB secretion by examining the expression of gap junction protein Cx43 in control, *Notch2/3* and *Rbpj* mutant P7 CBs. Cx43 has previously been shown to be required in the CB for controlling aqueous and vitreous humor secretion and thus maintaining the vitreous and IOP (Calera et al., 2006; Calera et al., 2009). As previously reported for the wild-type CB (Calera et al., 2006; Calera et al., 2009), Cx43 protein highly accumulates at the ICE-OCE apical junction, and the OCE express it at higher levels than the ICE (Fig. 5A–A'). In the OCE, Cx43 protein is also localized to the lateral cytoplasmic membrane. In contrast, *Notch2/3* and *Rbpj* mutant P7 CBs show a dramatic and significant reduction of Cx43 accumulation at the lateral side of the OCE compared to the P7 control, and additionally, apical ICE-OCE junctional accumulation also shows some degree of downregulation (Fig. 5B–D). Our mRNA FISH results show that *Cx43* mRNA is expressed in both the ICE and the OCE of the control CB, and their levels remain largely unchanged in both the epithelial layers of the *Notch2/3* and *Rbpj* mutant CBs (Fig. 5E–H). However, the OCE expresses much higher Cx43 proteins than the ICE, suggesting that Cx43 expression is regulated at the translational or posttranslational level. Taken together, these results suggest that NOTCH signaling regulates Cx43 protein levels and cellular localization in the OCE.

Since *Notch2/3* and *Rbpj* mutant eyes degenerate at the adult stage, we also examined the Cx43 expression in control and mutant adult CBs. In the adult control CB, Cx43 protein also accumulate at both the apical and lateral sides of the OCE, exhibiting similar expression and localization patterns to those at P7 (Fig. 5A and 5I). As at P7, the adult *Notch2/3* and

Rbpj mutant CBs show significantly lower Cx43 protein accumulation at the lateral side of the OCE, and its accumulation at the ICE-OCE apical junction also appears to decrease (Fig. 5I–L). These continuous downregulation of Cx43 protein in the adult *Notch2/3* or *Rbpj* mutant OCE might help explain low IOP, vitreous loss and eye degeneration.

Nectin1 stabilizes and localizes Cx43 protein in the OCE through direct interaction

Next, we investigated if NOTCH signaling maintains Cx43 protein in the OCE via Nectin1. In the control CB, Nectin1 is colocalized with Cx43 protein at both the apical and lateral sides of the OCE (Fig. 6A–A'). In addition, Nectin1 and Cx43 accumulation at the lateral side of the OCE almost diminishes in the *Rbpj* mutant CB (Fig. 6B–B'). Interestingly, forced *Nectin1* expression in the *Rbpj* mutant CB can drastically restore Cx43 accumulation at both apical and lateral sides of the OCE, suggesting that Nectin1 is important for Cx43 accumulation and lateral localization in the OCE (Fig. 6C–C'). As predicted, forced *Nectin1* expression in the *Rbpj* mutant CBs can also significantly restore the vitreous body, indicating that the loss of Nectin1 expression contributes to the shrinkage of the vitreous body in the developing *Rbpj* mutant eye (Fig. 6D–G). These results indicate that NOTCH signaling-regulated Nectin1 expression in the OCE is critical for maintaining Cx43 expression and thus the vitreous body.

Then, we investigated if Cx43 protein is directly associated with Nectin1 in P7 CBs. Cx43 can bring down Nectin1 protein efficiently from P7 CB protein extracts, suggesting that Cx43 form a protein complex with Nectin1 *in vivo* (Fig. 6H). In addition, Flag-tagged Nectin1 can also precipitate Cx43 protein in human 293T cells, further supporting that Nectin1 is associated with Cx43 protein (Fig. 6I). Moreover, the purified bacterially expressed GST-Cx43 C-terminal cytoplasmic domain, but not GST alone, can pull down His-tagged Nectin1 intracellular domain *in vitro*, indicating that the Nectin1 intracellular domain directly binds to the C-terminal cytoplasmic domain of Cx43 (Fig. 6J). Finally, Nectin1 overexpression can significantly stabilize Cx43 protein in human 293T cells (Fig. 6K). These results show that Nectin1 directly binds and stabilizes Cx43 protein, which can mechanistically explain why NOTCH signaling regulates the stabilization and cellular localization of Cx43 protein in the OCE.

NOTCH signaling directly controls the expression of the known vitreous protein Optc

Human and mouse CBs are known to express vitreous proteins, such as Optc (Hobby et al., 2000; Takanosu et al., 2001). Then, we used immunostaining to examine the expression of Optc protein in the *Notch2/3* double and *Rbpj* mutant P7 and adult CBs. Optc belongs to the extracellular matrix protein family of the small leucine rich repeat proteins (SLRPs), and a major vitreous protein component known to regulate the formation of collagen fibrils (Takanosu et al., 2001). In both the control P7 and adult CBs, Optc protein is highly expressed in the posterior ICE and also accumulates on the surface of the CB, the retina and the lens (Fig. 7A and 7B). By contrast, Optc expression is significantly downregulated in the *Notch2/3* double and *Rbpj* mutant P7 and adult CBs, indicating that NOTCH signaling controls Optc expression (Fig. 7C–G). Then, our mRNA FISH results have further shown that *Optc* mRNA exhibits the anterior-to-posterior gradient expression pattern in the ICE, and its expression in the ICE is significantly reduced in the *Rbpj* mutant CB compared to

the control CB (Fig. 7H–K). Our bioinformatics analysis has identified 6 consensus RBPJ binding sites in the *Optc* gene region (Fig. 7L). Our ChIP-qPCR results on the isolated CBs show that RBPJ indeed significantly occupies two of the predicted RBPJ binding sites in *Optc* (one in the promoter and one in the first intron), suggesting RBPJ directly regulates *Optc* transcription (Fig. 7L). In addition, the mouse CB is known to express *Col9a1*, *Col9a2* and *Col9a3*, which encode the heterotrimers of type IX fibrillar collagen in the vitreous (Dhawan and Beebe, 1994; Skeie et al., 2015). Our RNA FISH results have confirmed their expression in the ICE of the P7 CB, and have further shown that only *Col9a3* mRNA, but not *Col9a1* and *Col9a2* mRNAs, is significantly downregulated in the ICE of the *Rbpj* mutant CB (Fig. S7). Taken together, these results indicate that NOTCH signaling is critical for controlling the expression of the vitreous proteins in the ICE, including Optc and Col9a3.

RBPJ is required in the CB for the development of the cornea, the lens and the retina

To uncover the potential cause for *Rbpj* mutant eye degeneration, we then determined if different cell types contacting aqueous and vitreous humor undergo structural and protein expression changes in P14 control and *Rbpj* mutant eyes. In the P14 control cornea, collagen IV (ColIV) protein is expressed in endothelial cells, whereas Vimentin protein is expressed highly in stroma cells but less in endothelial cells (Fig. S8A–A'"). In contrast, the P14 *Rbpj* mutant eye upregulates Vimentin and downregulates ColIV in endothelial cells (Fig. S8A–B'"). In contrast to those in the control P14 eye, the Vimentin-positive lens epithelial cells in the P14 *Rbpj* mutant eye have undergone cuboid-to-columnar shape changes (Fig. S8C–E). Compared to the control, the central retina of the P14 *Rbpj* mutant eye significantly decreases the thickness of outer nuclear layer (ONL), photoreceptor outer segment (OS), inner nuclear layer (INL), inner plexiform layer (IPL: the processes of GCL and INL neurons), but not outer plexiform layer (OPL: the processes of photoreceptors and bipolar cells) and ganglion cell layer (GCL) (Fig. S8G and S8H). Calretinin-positive retinal ganglion cells (RGC) and amacrine cells (ACs) extend their processes into the IPL to form three distinct layers of synapses (Fig. S8I and S8I'). Interestingly, the distances between the synaptic layers are decreased in the *Rbpj* mutant eye compared to the control (Fig. S8I–J'). In addition, the *Rbpj* mutant eye also shows the abnormal distribution of Rhodopsin protein, a light-sensitive protein important for visual transduction, in the cell body and OS of rod photoreceptors compared to the control, suggesting that RBPJ is required in the RPE for photoreceptor development (Fig. S8K–L'). This is consistent with the previous finding that the RPE is important for photoreceptor development and OS formation (Sparrow et al., 2010; Fuhrmann et al., 2014). Taken together, NOTCH signaling in the CB might be important for the development or maintenance of corneal endothelial cell, lens epithelial cells and possibly RGC/AC neurons.

Discussion

So far, BMP and NOTCH2 signaling pathways have been shown to control CB morphogenesis (Chang et al., 2001; Sarode et al., 2014; Zhao et al., 2002; Zhou et al., 2013). Inactivating NOTCH downstream transcription factor RBPJ, but not NOTCH2, in the CB results in low IOP and eye degeneration, whereas constitutive NOTCH signaling

in the CB leads to high IOP (Sarode et al., 2014; Zhou et al., 2013). However, it remains unclear how NOTCH signaling controls CB development and secretion molecularly. In this study, we show that NOTCH2 and NOTCH3 function redundantly through RBPJ to regulate ICE-OCE adhesion, drive CB morphogenesis and directly control CB secretion, thereby maintaining IOP, the vitreous body and other eye tissues. NOTCH signaling controls CB morphogenesis and ICE-OCE adhesion by controlling *Nectin1* and *Nectin3* expression in the OCE. In addition, Nectin1 directly binds and stabilizes Cx43 protein in the OCE and localizes it at the lateral side of the OCE to promote aqueous humor secretion, thus maintaining the vitreous body and IOP. Moreover, NOTCH signaling in the ICE directly controls the expression of vitreous proteins, including Optc. Finally, NOTCH signaling is required in the RPE for maintaining photoreceptors as well as in the CB (and possibly the iris) for supporting cornea, lens and retinal development and maintenance, which mechanistically explains the requirement of NOTCH signaling in the CB for maintaining adult eye structures. Therefore, this study has significantly advanced our understanding of how canonical NOTCH-RBPJ signaling controls CB morphogenesis and secretion molecularly (Fig. 7M). NOTCH signaling is the first pathway identified so far for controlling CB secretion. Our findings have uncovered the importance of the CB in maintaining the vitreous body and supporting the development and maintenance of other eye tissues, and have also potentially revealed the mechanisms underlying eye diseases, including glaucoma, cataracts and cornea diseases.

NOTCH signaling controls ICE-OCE adhesion and CB morphogenesis by controlling Nectin expression in the OCE

Our findings demonstrate that NOTCH2 and NOTCH3 function redundantly to control ICE-OCE adhesion and CB morphogenesis by activating the expression of new NOTCH targets, *Nectin1* and *Nectin3*, in the OCE (Fig. 7M). First, NOTCH2 and NOTCH3 function redundantly to activate NOTCH signaling in the OCE. *Notch2/3* and *Dll1/Jag1* mRNAs are highly expressed in the OCE and the ICE, respectively, which supports our previous finding that Jag1 and Notch2 proteins are highly expressed in the ICE and OCE, respectively (Zhou et al., 2013). Importantly, *Notch2/3* and *Rbpj* mutant CBs show significantly lower *Hes1* expression in the OCE than *Notch2* or *Notch3* mutant CBs. Second, NOTCH2 and NOTCH3 function redundantly to promote ICE-OCE adhesion and CB morphogenesis as well as to maintain the vitreous body and IOP. *Notch2/3* double and *Rbpj* mutant developing CBs, but not *Notch2* and *Notch3* mutant ones, exhibit defective ICE-OCE adhesion, and cause smaller vitreous and lower IOP in the eye as well as eye degeneration. Since the *Rbpj* mutant CB causes much more severe eye phenotypes than the *Notch2/3* mutant ones but they affect NOTCH signaling similarly, RBPJ might have NOTCH signaling-independent functions in the CB, which has been proposed in other developmental contexts (Johnson and Macdonald, 2011). In the future, it will be important to uncover NOTCH-independent functions of RBPJ in the CB. Third, NOTCH signaling directly activates *Nectin1* expression in the OCE to promote ICE-OCE adhesion, CB morphogenesis and vitreous formation. Nectin1 in the OCE is engaged to Nectin3 in the ICE to control CB morphogenesis, but its regulation in the CB remains unclear (Inagaki et al., 2005). *Notch2/3* and *Rbpj* mutant CBs significantly decrease the expression of *Nectin1 mRNA* and protein in the OCE, and exhibit the loss of apical accumulation of Nectin3 protein in the ICE likely due to decreased

Nectin1 in the OCE. Additionally, RBPJ directly binds to the promoter region of *Nectin1 in vivo*. Furthermore, forced *Nectin1* expression in the *Rbpj* mutant CB can partially restore ICE-OCE adhesion, CB morphogenesis and the vitreous size, suggesting that Nectin1 is a major NOTCH target in the CB, but other important targets also exist. Taken together, this study provides important insight into how NOTCH signaling controls CB development (Fig. 7M). Similarly, NOTCH2 and NOTCH3 are known to regulate mouse vascular development and control human trophoblast cell proliferation (Wang et al., 2012; Zhao et al., 2017). Because of their wide co-expression in various developing and adult mammalian tissues, their functional redundancy is likely a common phenomenon.

NOTCH signaling in the CB maintains the vitreous by regulating Nectin-mediated Cx43 stabilization/localization in the OCE and the expression of vitreous proteins in the ICE

The CB is known to be responsible for secreting the aqueous humor in the anterior chamber, and the vitreous humor and protein components, including crystallin, Optc, collagen and laminin proteins (Coca-Prados and Escribano, 2007; Delamere, 2005). Cx43-formed gap junctions in the CB are known to control aqueous and vitreous humor production and thus maintain the vitreous and IOP, but the regulation of Cx43 in controlling CB secretion remains unknown (Calera et al., 2006; Calera et al., 2009). This study demonstrates that the NOTCH-Nectin1 axis is important for stabilizing and localizing Cx43 in the OCE, thereby controlling aqueous and vitreous humor secretion (Fig. 7M). First, NOTCH signaling controls aqueous and vitreous humor secretion in the mouse eye. *Notch2/3* and *Rbpj* mutant developing and adult eyes have smaller vitreous body and lower IOP than control ones, which is consistent with the finding on *Mart1-Cre*-mediated *Rbpj* deletion in the CB (Sarode et al., 2014). Second, NOTCH signaling stabilizes and localizes Cx43 protein in the OCE. *Notch2/3* and *Rbpj* mutant developing or adult OCEs significantly decrease Cx43 protein and lateral accumulation, which severity is closely related to the defects in the IOP, the vitreous and eye structures, supporting a key role of Cx43 in vitreous and aqueous humor secretion. *Cx43* mRNA expression is not changed in the *Notch2/3* or *Rbpj* mutant CB, suggesting that NOTCH signaling controls Cx43 expression at the translational or posttranslational level. Third, Nectin1 stabilizes and laterally localizes Cx43 in the OCE through direct interaction. *Nectin1* mutant eyes also have the severe loss of the vitreous, but the underlying mechanism remains unclear (Inagaki et al., 2005). Forced *Nectin1* expression can restore Cx43 expression and lateral localization in the OCE of the *Rbpj* mutant CB. Nectin1 directly interacts with and stabilizes Cx43 protein in cultured human 293 cells. It is worth pointing out that the surface area loss of the *Notch2/3* or *Rbpj* mutant CB should also contribute to the secretion defect. Therefore, this study demonstrates that NOTCH signaling-regulated Nectin1 directly interacts with, stabilizes and subcellularly localizes Cx43 protein in the CB for controlling aqueous and vitreous humor secretion, providing important insight into how NOTCH signaling maintains the vitreous and IOP (Fig. 7M).

The ICE in humans and mice secrete vitreous proteins, including Optc and collagen proteins, but how their expression is regulated molecularly in the ICE remains unknown (Bishop et al., 2002; Takanosu et al., 2001). This study has, for the first time, shown that NOTCH signaling directly controls the expression of vitreous proteins in the ICE (Fig. 7M). NOTCH2/3-mediated canonical signaling is active in the ICE based on *Hes1* expression.

Compared to the control CBs, the *Notch2/3* and *Rbpj* mutant CBs significantly decrease *Optc* and *Col9a3* mRNAs. In addition, RBPJ directly occupies the regulatory regions of *Optc* in the CB *in vivo*. Furthermore, NOTCH signaling-regulated CB secretion is critical for the development or maintenance of the cornea, the lens and possibly the retina since the *Rbpj* mutant eye exhibits the defects in cornea endothelial cells, lens epithelial cells and retinal neurons. Therefore, this study has uncovered an important role of canonical NOTCH signaling in the regulation of vitreous protein production (Fig. 7M). In the future, it will be important to investigate how CB-secreted vitreous proteins contribute to the development and maintenance of various eye structures as well as the pathogenesis of eye diseases.

STAR★Methods

Resource Availability

Lead Contact—Further information and requests for resources and reagents should be directed to and will be fulfilled by the Lead Contact, Ting Xie (tgx@stowers.org).

Materials Availability—New reagents generated in this study are available via the lead contact.

Data and Code Availability—No datasets were generated during this study. Original data underlying this manuscript can be accessed from the Stowers Original Data Repository at http://www.stowers.org/research/publications/libpb-xxxx.

Experimental Model and Subject Details

Mouse strains—All mice were housed and cared according to the ARVO Statement for the Use of Animals in Ophthalmic and Vision Research and guidelines of the Institutional Animal Care and Use Committees at the Stowers Institute for Medical Research. *C57BL/6J*, *Z/EG*, *CBA/CaJ*, *C57BL/10J* and *CD-1* strains are provided by the Lab Animal Service Facility of Stowers Institute for Medical Research. *Tyrp1-Cre*, *Tyrp2-Cre*, *Notch2*$^{fx/fx}$, *Notch3*$^{-/-}$ and *Rbpj*$^{fx/fx}$ strains were previously described (Davis et al., 2009; Krebs et al., 2003; McCright et al., 2006; Mori et al., 2002; Tanigaki et al., 2002). The conditional *Nectin1* overexpression strain was generated by the Lab Animal Service Facility of Stowers Institute for Medical Research. For all the experiments, both male and female mice at the age of P3 to adult (2–12 months old) were used.

Cell Lines—293T Cell lines were purchased from ATCC (American Type Culture Collection) and cultured as recommended.

Method Details

Genotyping—Genotyping was performed on mouse tail or ear clips by Transnetyx Inc or by the Xie lab. For genotyping by the Xie lab, the mouse genome DNA was extracted by heating each tail or ear clip in 0.1 ml solution A (25 mM NaOH/0.2 mM EDTA) at 95 °C for 1 hour. The solution was then centrifuged briefly and neutralized by 0.1 ml solution B (40mM Tris-HCl) before being used for the PCR template. PCR amplification of the desired

DNA fragments was performed according to the protocol of GoTaq G2 Green Master Mix (M7823, Promega Corporation). The primers used for genotyping are listed in Table S1.

Intraocular pressure (IOP) measurement—Adult mice older than 2 months were measured for IOP. The mice were first anesthetized with Ketamine (100 mg/kg) /Xylazine (10 mg/kg), and IOP was determined by the mean of six consecutive measurements by TonoLab rebound tonometer (Icare, Helsinki, Finland). Male and female mice were both tested.

Tissue preparation for cryosections, paraffin sections and plastic sections —Eyes were enucleated and fixed immediately after euthanasia. For paraffin or plastic sections, eyeballs were fixed by immersion in Hartman's Fixative (H0290, Sigma-Aldrich) for 20 hours and then in 4% paraformaldehyde in 1xPBS (J19943-K2, Thermo Fisher Scientific) for 20 hours at room temperature. The fixed eyeballs were then rinsed in 1x PBS, dehydrated through graded ethanol (30%, 50%, 70%; 1 hour in ambient every step) and then proceeded for paraffin or plastic embedding. The samples for paraffin-embedding were further dehydrated through graded ethanol (85% and 95%; 1 hour in ambient every step) before they were processed with a PATHOS Delta hybrid tissue processor (Milestone Medical Technologies). The samples for plastic-embedding were further dehydrated in 100% ethanol and embedded following the protocol of the 'Immuno-Bed' kit (#17324–1, Polysciences). 5 μm paraffin or plastic sections were cut using a Leica RM2255 microtome (Leica Biosystems Inc) and mounted on Superfrost Plus microscope slides (12–550-15, Thermo Fisher Scientific) or SureBond charged microscope slides (SL6332–1, Avantik).

For cryosections, the eyeballs were fixed in 4% paraformaldehyde in 1xPBS (J19943-K2, Thermo Fisher Scientific) for an overnight in 4 °C. The samples were then rinsed in PBS, dehydrated in gradient sucrose solution (15% and 30% in 1x PBS in 4 °C for an overnight) and flash frozen in Tissue-Tek OCT medium (Cat#4583, SAKURA FINETEK USA Inc) in liquid nitrogen. Cryo-sections were cut at the thickness of 12 μm and mounted on Superfrost Plus microscope slides (12–550-15, Thermo Fisher Scientific) or SureBond charged microscope slides (SL6332–1, Avantik).

For de-paraffinization, prepared sections were heated at 60°C for 60 minutes and washed in xylene (three changes, 5 minutes for each change) and subsequently in ethanol (three changes, 5min for each change). For H&E staining, the 5 μm deparaffinized sections or plastic sections were rehydrated in 80% ethanol and rinsed in tap water. The sections then went through a standard H&E staining protocol using the Leica AutoXL automatic stainer and the Leica ST Infinity staining system (3802098, Leica), and were then mounted by Surgipath Micromount (3801730, Leica) for further imaging and morphological analysis.

Immunofluorescent staining—Immunofluorescent staining was performed as previously described (Zhou et al., 2013). Briefly, before the antigen retrieval, the deparaffinized sections and OCT-removed cryosections were air dried in ambient for 20 minutes. The tissue sections were then heated in 1x citrate buffer (pH=6.0) in 95°C for 10 minutes for antigen retrieval and then rinsed by1x PBS (three changes, 5 minutes each) in ambient. The sections were blocked by 1x Power Block (HK085–5K, Biogenex

Laboratories). Primary antibody was diluted in 1x Power Block solution and the sections were incubated with primary antibody at 4 °C overnight. After the sections were washed by 1x PBS (three changes, 5 minutes each), secondary antibody incubation was performed at ambient for 1 hour. Primary and secondary antibodies are listed in Key Resources Table. For Nectin1 staining, incubation with 1x Rabbit-on-Rodent HRP-Polymer (RMR622L, BioCare Medical) for 30 minutes for replacing secondary antibody labeling. The sections were then incubated with TSA-plus Fluorescein system (NEL741001KT, PerkinElmer) for 20 minutes after 1x PBS wash (three changes, 5 minutes each). DAPI counter-staining was performed with 2 μg/ml DAPI (D9542, Sigma-Aldrich) in 1xPBS for 15-minute incubation. The prepared sections were mounted by ProLong™ Glass Antifade Mountant (P36980, Thermo Fisher Scientific) or Vectashield Mounting Medium for Fluorescence (H-1000, Vector Laboratories) for further imaging.

EdU (5-ethynyl-2 deoxyuridine) labeling—For EdU labeling, EdU (TCI) was injected into pups through intraperitoneal injection at the dosage of 0.1 mg/g body weight 3 hours before the eyes were enucleated. Eye samples were fixed and paraffin-embedded, sectioned and de-paraffinized as described earlier. De-paraffinized sections were then labeled following the protocol of Click-iT™ EdU Alexa Fluor™ 488 Imaging Kit (#C10337, Thermo Fisher Scientific). Briefly, sections were blocked by 1x Power Block and then incubated with Click-iT® reaction cocktail (1x Click-iT® reaction buffer, 1x CuSO4, 1xAlexa Fluor® azide and 1xReaction buffer additive) at ambient for 30 minutes. The cocktail was then removed, and the sections were washed by 1x Power Block and PBS before further antibody and/or DAPI staining.

RNA fluorescent in situ hybridization (FISH)—RNA FISH was performed on paraffin sections utilizing viewRNA cell plus assay kit (88–19000-99, Thermo Fisher Scientific). Briefly, the deparaffinized sections were air dried at ambient for 20 minutes before they were treated with 3% hydrogen peroxide in 1x Tris buffer (pH=8.0) for 15 minutes, heated at 99°C for 15 minutes in 1x citrate buffer (pH=6.0) and digested with 1:500 protease QF (Thermo Fisher Scientific, QVT0512) in 1x PBS for 10 minutes at ambient. Hybridization was carried out in a humid box at 40°C overnight. Excess probe sets were washed with 1x wash buffer (2 changes, 5 minutes for each change), 0.5x SSC with 0.1% Triton (2 changes, 10 minutes each), 1x wash buffer (2 changes, 5 minutes each) after the hybridization. The probe sets used for FISH in this study are listed in the Key Resources Table. For signal amplification and detection, sections were incubated with preamplifier solution, amplifier solution and label probe mix solution for 1 hour at 40 °C, respectively, with washing with 1x wash buffer (2 changes, 5 minutes each), 0.5x SSC with 0.1% Triton (2 changes, 10 minutes each), 1x wash buffer (2 changes, 5 minutes each) performed between each two incubation. The sections were counter-stained with 10 μg/ml DAPI in 1x wash buffer for 15 minutes, and excess DAPI was washed away with 0.5X SSC containing 0.1% Triton X (2 changes, 10 minutes each) and 1xPBS (2 changes, 5 minutes each). Trueview AF Quenching Kit (SP-8400–15, Vector Laboratories) was applied to the sections followed by 1xPBS wash (2 changes, 5 minutes each). The prepared sections were mounted by ProLong™ Glass Antifade Mountant (P36980, Thermo Fisher Scientific) for further imaging.

Microscopy and quantification—Sections with H&E staining were imaged by Olympus VS120 slide scanner (Olympus) using a 20x air objective, and the sections from immunofluorescence and RNA FISH were imaged by Leica TCS SP5 (Leica) using a 40x or 63x oil objective. All the analysis on fluorescent intensity in the confocal images were performed using Fiji and custom written macros. Prior to the analyses, raw images were processed by subtracting background, and were then projected for the max intensity to form single multiple-color images. All the ROIs at either the region of OCE or ICE were manually drawn based on the bright-field images. Cx43 and OPTC quantifications are based on the intensity per area and are further normalized by the average intensity per area of the WT. For RNA FISH images, to better visualize weak signal, a non-linear histogram adjustment (gamma =0.3) was applied to the DAPI channel to increase the visibility of the nuclei of OCE cells whose fluorescent signals were masked by black pigments. For better visualization, a gaussian blur (sigma =0.8~1.2, mRNA target dependent and sigma=2.0 for DAPI) was applied to every channel. Individual RNA spot was identified by Fiji internal function “Find Maxima” and then chose “single points” as the output. The total number of spots at each fluorescence channel was quantified and saved using the custom written macro.

Chromatin immunoprecipitation and quantitative PCR (ChIP-qPCR)—ChIP was performed based on the protocol of Pierce™ Agarose ChIP Kit (26156, Thermo Fisher Scientific). Briefly, thirty ciliary bodies manually dissected from P7 CD-1 mouse eyes were crosslinked with 1% formaldehyde at room temperature for 10 minutes, and 0.125 M glycine was added to stop the reaction by incubation at room temperature for 5 minutes, followed by washing twice with ice-cold PBS containing protease inhibitor cocktail (PIC). The ciliary bodies were homogenized with homogenization buffer (10 mM Tris-HCl, pH 6.7, 10 mM KCl, 0.15 mM $MgCl_2$, 1 mM PMSF, and 1 mM DTT, with PIC) in a Dounce homogenizer with Teflon pestle (Wheaton, Thomas Scientific). The nuclei were recovered by centrifuging and resuspended in the cell nuclear lysis buffer containing PIC. The cell pellet was collected and resuspended in the MNase digestion buffer. Chromatin was fragmented by Micrococcal Nuclease (ChIP Grade) to 200–500 bp in length. The digested chromatin was centrifuged at 9,000 g, 4°C for 15 minutes, transferred to a new 1.5 mL eppendorf tube, and added with 100 ul of the complete ChIP buffer. 1/10 volume (20 μl) was set aside as input control. The nuclear extracts were immunoprecipitated with 20μl ChIP-grade Protein A/G magnetic beads pre-conjugated with 10μg RBPJ antibody (Abcam) or normal rabbit IgG (Promega). Beads-DNA complexes were eluted at 65°C for 30 minutes in 150 μL of 1x IP elution buffer and transferred to a fresh tube. Samples were added with 6 μl 5M NaCl and 2 μl of 20 mg/ml Proteinase K, and incubated in a thermomixer at 1300 rpm, 65°C for 1.5 hours. Immunoprecipitated DNA was purified by phenol chloroform extraction and resolved in 50 μL sterilized distilled water. ChIP-qPCR reactions were performed using SYBR Green PCR master mix kit as previously described (Zhou et al., 2013). The mouse negative control primer was purchased from Active Motif: Enabling Epigenetics Research (USA). The primers used for ChIP-qPCR in this study are shown in Table S2.

Generation of CAG>STOP>Nectin1-Flag—The coding region of *Nectin1* cDNA was amplified first using two primers (Forward: cctcctggcagccccttcg; Reverse: ggggaagggtgggtgaggga). Since the coding region contains an internal EcoRI

restriction site, the site was mutated by overlapping PCR. The mutated Nectin1 coding region was then amplified using a primer containing an EcoRI site (gatggaattcgctcggatggggcttgcgggcgc) and the other primer carrying an EcoRI site and a Flag tag (aggtgaattcttacttatcgtcgtcatccttgtaatccacataccactctttcttgga). The PCR product was digested and cloned into the only EcoRI site after the second LoxP site in the pMES>STOP> EcoRI-IRES-GFP vector. Finally, the mutated EcoRI site was mutated back by site-directed mutagenesis. The linearized DNA was injected into fertilized (*CBA/CaJ x C57BL/10J*) F1 embryos by pronuclear injection. Three founder lines were established by crossing with *C57BL/6*, and only two founder lines produced litters expressing both Flag and GFP. The progeny from one of the two founder lines were used for rescue experiments.

Protein co-immunoprecipitation (co-IP), Western blotting and *in vitro* protein binding—Human 293T cell line was obtained from the American Type Culture Collection (ATCC) and cultured as recommended. The cells were cultured with 90% DMEM+ 10% heat inactivated FBS. All procedures involving human cell lines were approved by the Institutional Biosafety Committee (IBC) of Stowers Institute for Medical Research. The membrane proteins of 293T cells transfected with *pCMV6-Myc-Nectin1* or mouse CBs of CD1 strains were extracted by the Mem-PER™ Plus Membrane Protein Extraction Kit (ThermoFisher Scientific), and then the membrane proteins were used for co-IP to determine the interaction between Nectin1 and Cx43. Protein A beads (Bio processing CaptivA PriMAB, Cat CA-PRI-0100 Waltham, Massachusetts, USA) were coupled with the antibodies against Cx43 or Flag from the membrane protein extracts. Two control IPs were done by employing protein A beads alone with the membrane protein extract (NE) or the specific antibodies (Ab). Input proteins for co-IPs were membrane protein lysates from mouse CBs or 293T cells. 1mg protein was used in each co-IP. Protein A agarose bead volumes were scaled down to 50 μL (antibody: bead ratio was maintained). Cell lysates or samples from co-IP were separated by NuPAGE 4%–12% Bis-Tris Protein Gel (Invitrogen) in NuPAGE MES SDS Running Buffer (Invitrogen) according to different protein size. Proteins were electrophoretically transferred to a nitrocellulose membrane (Thermo) with NuPAGE Transfer Buffer (Invitrogen). Blots were blocked for 1 hour at room temperature in 1x PBS-T + 5% fat-free milk according to antibody requirements and probed overnight at 4°C with primary antibodies against Cx43, Nectin 1, Flag or β-actin. After washing three times in 1x PBS-T, signals were detected by using secondary mouse or rabbit antibodies conjugated to horseradish peroxidase. Secondary antibodies were incubated for 1 hour at room temperature. After three times washes, a SuperSignal™ West Dura Extended Duration substrate detection kit (Thermo) was used to expose the signals to the high-resolution Biomax MR films (Carestream).

The interaction between Cx43 and Nectin1 was verified by GST pulldown assay *in vitro*. The plasmids pGEX-4T1/Cx43-C-terminal (257–382) and pET28a/Nectin1-C-terminal (313–515) were constructed for expressing GST-Cx43 and His-Nectin1, respectively. GST-CX43 and His-Nectin1 were expressed in *E. coli* and purified by Pierce™ Glutathione Agarose and HisPur™ Ni-NTA Superflow Agarose (ThermoFisher Scientific), respectively. 100 μg of GST-CX43 and His-Nectin 1 were used in each GST pulldown group. Glutathione agarose bead volumes were scaled down to 50 μL and run on 4–12% Bis-Tris gel

(Invitrogen). Samples were visualized by GelCode™ Blue Stain Reagent (ThermoFisher Scientific).

Quantification and statistical analysis

Imaging pre-processing and measurement were all performed in Fiji. ANOVA was first used to determine if there are any significant differences among multiple groups. If the *P*-value for the ANOVA test is less than 0.05, two-tailed Student's test was also used to determine the *P* values for pair-wise comparisons. All data are expressed as mean ± SEM (the standard error of the mean).

Supplementary Material

Refer to Web version on PubMed Central for supplementary material.

Acknowledgements

We would like to thank P. Chambon, T. Gridley, L. Li and P. Trainor for providing reagents. We would also like to thank the Stowers facilities for superb technical support, and the Xie laboratory members for stimulating discussion. This work was supported by National Eye Institute (EY027441, T. X.), Stowers Institute for Medical Research (T. X) and a scholarship by China Scholarship Council (J. P.).

References

Andersson ER, Sandberg R, and Lendahl U (2011). Notch signaling: simplicity in design, versatility in function. Development 138, 3593–3612. [PubMed: 21828089]

Beebe DC (1986). Development of the ciliary body: a brief review. Trans Ophthalmol Soc U K 105 (Pt 2), 123–130. [PubMed: 3541302]

Bishop PN, Takanosu M, Le Goff M, and Mayne R (2002). The role of the posterior ciliary body in the biosynthesis of vitreous humour. Eye (Lond) 16, 454–460. [PubMed: 12101453]

Calera MR, Topley HL, Liao Y, Duling BR, Paul DL, and Goodenough DA (2006). Connexin43 is required for production of the aqueous humor in the murine eye. J Cell Sci 119, 4510–4519. [PubMed: 17046998]

Calera MR, Wang Z, Sanchez-Olea R, Paul DL, Civan MM, and Goodenough DA (2009). Depression of intraocular pressure following inactivation of connexin43 in the nonpigmented epithelium of the ciliary body. Invest Ophthalmol Vis Sci 50, 2185–2193. [PubMed: 19168903]

Chang B, Smith RS, Peters M, Savinova OV, Hawes NL, Zabaleta A, Nusinowitz S, Martin JE, Davisson ML, Cepko CL, et al. (2001). Haploinsufficient Bmp4 ocular phenotypes include anterior segment dysgenesis with elevated intraocular pressure. BMC Genet 2, 18. [PubMed: 11722794]

Cho SH, and Cepko CL (2006). Wnt2b/beta-catenin-mediated canonical Wnt signaling determines the peripheral fates of the chick eye. Development 133, 3167–3177. [PubMed: 16854977]

Coca-Prados M, and Escribano J (2007). New perspectives in aqueous humor secretion and in glaucoma: the ciliary body as a multifunctional neuroendocrine gland. Prog Retin Eye Res 26, 239–262. [PubMed: 17321191]

Curtin BJ (1979). Physiologic vs pathologic myopia: genetics vs environment. Ophthalmology 86, 681–691. [PubMed: 397448]

Davis N, Mor E, and Ashery-Padan R (2011). Roles for Dicer1 in the patterning and differentiation of the optic cup neuroepithelium. Development 138, 127–138. [PubMed: 21138975]

Davis N, Yoffe C, Raviv S, Antes R, Berger J, Holzmann S, Stoykova A, Overbeek PA, Tamm ER, and Ashery-Padan R (2009). Pax6 dosage requirements in iris and ciliary body differentiation. Dev Biol 333, 132–142. [PubMed: 19563798]

Delamere NA (2005). Ciliary Body and Ciliary Epithelium. Adv Organ Biol 10, 127–148. [PubMed: 21234280]

Dhawan RR, and Beebe DC (1994). Differential localization of collagen type IX isoform messenger RNAs during early ocular development. Invest Ophthalmol Vis Sci 35, 470–478. [PubMed: 8112996]

Dias da Silva MR, Tiffin N, Mima T, Mikawa T, and Hyer J (2007). FGF-mediated induction of ciliary body tissue in the chick eye. Dev Biol 304, 272–285. [PubMed: 17275804]

Fuhrmann S, Zou C, and Edward M Levine, E.M. (2014). Retinal pigment epithelium development, plasticity, and tissue homeostasis. Exp Eye Res 0: 141–150.

Gage PJ, Rhoades W, Prucka SK, and Hjalt T (2005). Fate maps of neural crest and mesoderm in the mammalian eye. Invest Ophthalmol Vis Sci 46, 4200–4208. [PubMed: 16249499]

Hagglund AC, Jones I, and Carlsson L (2017). A novel mouse model of anterior segment dysgenesis (ASD): conditional deletion of Tsc1 disrupts ciliary body and iris development. Dis Model Mech 10, 245–257. [PubMed: 28250050]

Hobby P, Wyatt MK, Gan W, Bernstein S, Tomarev S, Slingsby C, and Wistow G (2000). Cloning, modeling, and chromosomal localization for a small leucine-rich repeat proteoglycan (SLRP) family member expressed in human eye. Mol Vis 6, 72–78. [PubMed: 10837509]

Inagaki M, Irie K, Ishizaki H, Tanaka-Okamoto M, Morimoto K, Inoue E, Ohtsuka T, Miyoshi J, and Takai Y (2005). Roles of cell-adhesion molecules nectin 1 and nectin 3 in ciliary body development. Development 132, 1525–1537. [PubMed: 15728677]

Janssen SF, Gorgels TG, Bossers K, Ten Brink JB, Essing AH, Nagtegaal M, van der Spek PJ, Jansonius NM, and Bergen AA (2012). Gene expression and functional annotation of the human ciliary body epithelia. PloS one 7, e44973. [PubMed: 23028713]

Jo AO, Lakk M, Frye AM, Phuong TT, Redmon SN, Roberts R, Berkowitz BA, Yarishkin O, and Krizaj D (2016). Differential volume regulation and calcium signaling in two ciliary body cell types is subserved by TRPV4 channels. Proc Natl Acad Sci U S A 113, 3885–3890. [PubMed: 27006502]

Johnson JE, and Macdonald RJ (2011). Notch-independent functions of CSL. Curr Top Dev Biol 97, 55–74. [PubMed: 22074602]

Krebs LT, Xue Y, Norton CR, Sundberg JP, Beatus P, Lendahl U, Joutel A, and Gridley T (2003). Characterization of Notch3-deficient mice: normal embryonic development and absence of genetic interactions with a Notch1 mutation. Genesis 37, 139–143. [PubMed: 14595837]

Kubo F, Takeichi M, and Nakagawa S (2003). Wnt2b controls retinal cell differentiation at the ciliary marginal zone. Development 130, 587–598. [PubMed: 12490564]

Kulic I, Robertson G, Chang L, Baker JH, Lockwood WW, Mok W, Fuller M, Fournier M, Wong N, Chou V, et al. (2015). Loss of the Notch effector RBPJ promotes tumorigenesis. J Exp Med 212, 37–52. [PubMed: 25512468]

Liu H, Xu S, Wang Y, Mazerolle C, Thurig S, Coles BL, Ren JC, Taketo MM, van der Kooy D, and Wallace VA (2007). Ciliary margin transdifferentiation from neural retina is controlled by canonical Wnt signaling. Dev Biol 308, 54–67. [PubMed: 17574231]

McCright B, Lozier J, and Gridley T (2006). Generation of new Notch2 mutant alleles. Genesis 44, 29–33. [PubMed: 16397869]

Morgan IG, Ohno-Matsui K, and Saw SM (2012). Myopia. Lancet 379, 1739–1748. [PubMed: 22559900]

Mori M, Metzger D, Garnier JM, Chambon P, and Mark M (2002). Site-specific somatic mutagenesis in the retinal pigment epithelium. Invest Ophthalmol Vis Sci 43, 1384–1388. [PubMed: 11980850]

Mumm JS, and Kopan R (2000). Notch signaling: from the outside in. Dev Biol 228, 151–165. [PubMed: 11112321]

Reis LM, and Semina EV (2011). Genetics of anterior segment dysgenesis disorders. Curr Opin Ophthalmol 22, 314–324. [PubMed: 21730847]

Sarode B, Nowell CS, Ihm J, Kostic C, Arsenijevic Y, Moulin AP, Schorderet DF, Beermann F, and Radtke F (2014). Notch signaling in the pigmented epithelium of the anterior eye segment promotes ciliary body development at the expense of iris formation. Pigment cell & melanoma research 27, 580–589. [PubMed: 24628886]

Schindelin J, Arganda-Carreras I, Frise E, Kaynig V, Longair M, Pietzsch T, Preibisch S, Rueden C, Saalfeld S, Schmid B, et al. (2012). Fiji: an open-source platform for biological-image analysis. Nat Methods 9, 676–682. [PubMed: 22743772]

Schneider CA, Rasband WS and Eliceiri KW (2012). NIH Image to ImageJ: 25 years of image analysis. Nat Methods 9, 671–675. [PubMed: 22930834]

Skeie JM, Roybal CN, and Mahajan VB (2015). Proteomic insight into the molecular function of the vitreous. PloS one 10, e0127567. [PubMed: 26020955]

Sparrow JR, Hicks D, and Hamel CP (2010). The retinal pigmented epithelium in health and disease. Curr Mol Med 10, 802–823. [PubMed: 21091424]

Stamer WD, and Acott TS (2012). Current understanding of conventional outflow dysfunction in glaucoma. Curr Opin Ophthalmol 23, 135–143. [PubMed: 22262082]

Takanosu M, Boyd TC, Le Goff M, Henry SP, Zhang Y, Bishop PN, and Mayne R (2001). Structure, chromosomal location, and tissue-specific expression of the mouse opticin gene. Invest Ophthalmol Vis Sci 42, 2202–2210. [PubMed: 11527931]

Tanigaki K, Han H, Yamamoto N, Tashiro K, Ikegawa M, Kuroda K, Suzuki A, Nakano T, and Honjo T (2002). Notch–RBP-J signaling is involved in cell fate determination of marginal zone B cells. Nature immunology 3, 443–450. [PubMed: 11967543]

Truett GE, Heeger P, Mynatt RL, Truett AA, Walker JA, and Warman ML (2000). Preparation of PCR-quality mouse genomic DNA with hot sodium hydroxide and tris (HotSHOT). Biotechniques 29, 52, 54. [PubMed: 10907077]

Wang H, Zou J, Zhao B, Johannsen E, Ashworth T, Wong H, Pear WS, Schug J, Blacklow SC, Arnett KL, et al. (2011). Genome-wide analysis reveals conserved and divergent features of Notch1/RBPJ binding in human and murine T-lymphoblastic leukemia cells. Proc Natl Acad Sci U S A 108, 14908–14913. [PubMed: 21737748]

Wang Q, Zhao N, Kennard S, and Lilly B (2012). Notch2 and Notch3 function together to regulate vascular smooth muscle development. PLoS One 7, e37365. [PubMed: 22615991]

Wang Y, Zheng Y, Chen D, and Chen Y (2013). Enhanced BMP signaling prevents degeneration and leads to endochondral ossification of Meckel's cartilage in mice. Dev Biol 381, 301–311. [PubMed: 23891934]

Yang J, Nan C, Ripps H, Shen W (2015). Destructive changes in the neuronal structure of the FVB/N mouse retina. PLoS ONE 10, e0129719. [PubMed: 26091175]

Zhang K, Zhang L, and Weinreb RN (2012). Ophthalmic drug discovery: novel targets and mechanisms for retinal diseases and glaucoma. Nat Rev Drug Discov 11, 541–559. [PubMed: 22699774]

Zhao WX, Wu ZM, Liu W, and Lin JH (2017). Notch2 and Notch3 suppress the proliferation and mediate invasion of trophoblast cell lines. Biol Open 6, 1123–1129. [PubMed: 28606936]

Zhao S, Chen Q, Hung FC, and Overbeek PA (2002). BMP signaling is required for development of the ciliary body. Development 129, 4435–4442. [PubMed: 12223402]

Zhou Y, Tanzie C, Yan Z, Chen S, Duncan M, Gaudenz K, Li H, Seidel C, Lewis B, Moran A, et al. (2013). Notch2 regulates BMP signaling and epithelial morphogenesis in the ciliary body of the mouse eye. Proc Natl Acad Sci U S A 110, 8966–8971. [PubMed: 23676271]

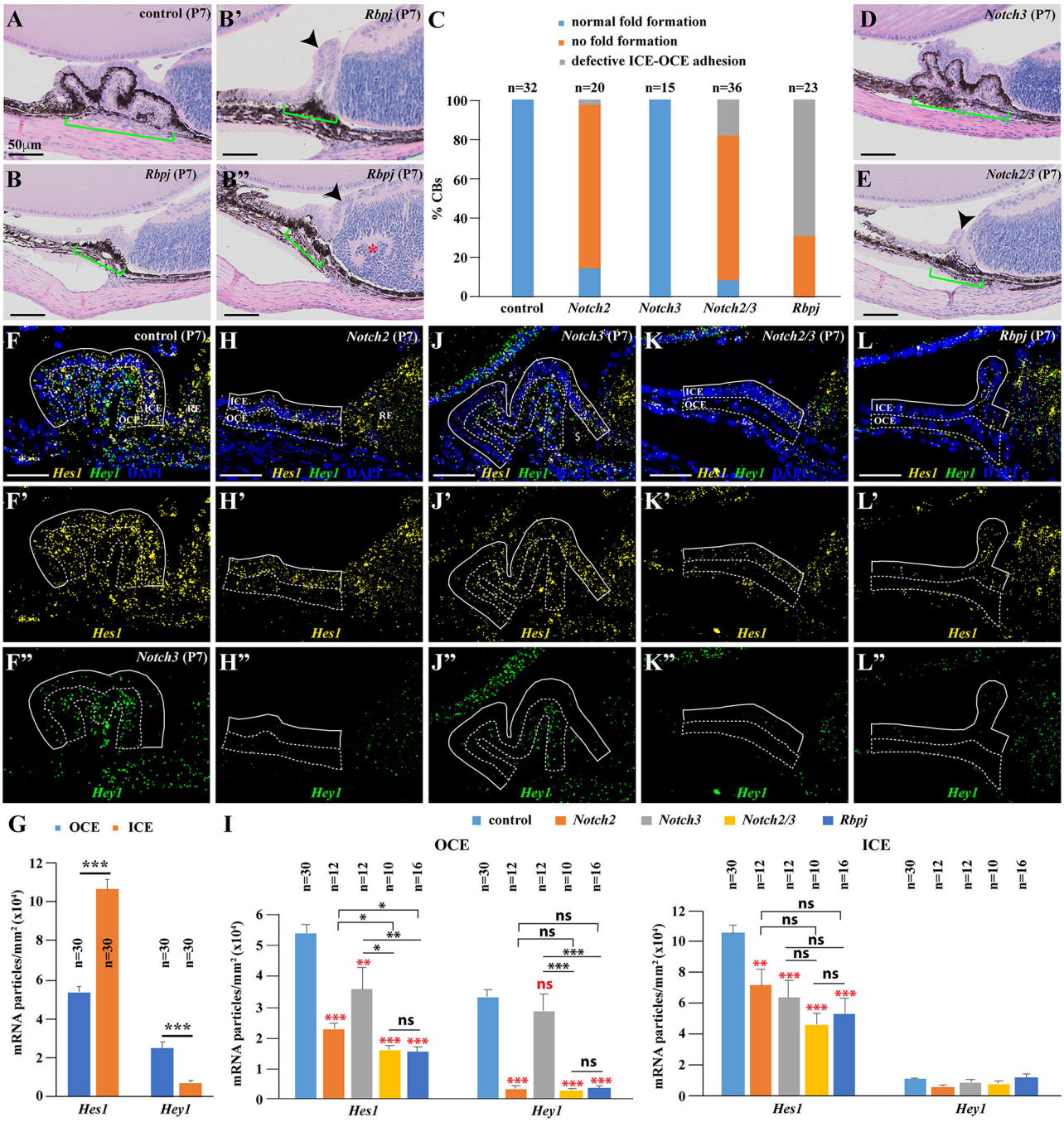

Figure 1. NOTCH2 and NOTCH3 function redundantly to signal via RBPJ for controlling ICE-OCE adhesion and CB morphogenesis.

Green brackets indicate CB regions, whereas arrowheads point to the OCE region separated from the ICE. **A–B”**, **D** and **E** are HE-stained sections, whereas **F–L”** are confocal sections. (**A–E**) P7 *Rbpj* mutant CBs show no CB folds (**B**) and ICE-OCE separation (**B’**: a epithelial stem formed by the separated OCE; **B”**: the separated OCE lying on the top of the retina), while a P7 *Notch2/3* double mutant CB exhibits the OCE stem (**E**), compared to a P7 control CB (**A**) and a P7 *Notch3* mutant CB (**D**) containing three folds. **C**: quantification results.

(**F-G**) mRNA FISH results show that *Hes1* is expressed in both the ICE and OCE of the control P7 CB but with higher levels in the ICE, whereas *Hey1* is primarily expressed in the OCE (**G**: quantification results). (**H–L”**) mRNA FISH results show that both *Notch2* and *Notch3* contribute to NOTCH signaling in both the ICE and OCE based on the expression of *Hes1* and *Hey1* mRNAs (**I**: quantification results). Red and black asterisks show control-vs-mutant and mutant-vs-mutant comparisons, respectively. Two-tailed Student’s t-test: *, $P<0.05$; **, $P<0.01$; ***, $P<0.001$; ns, no significance. Bars: 50μm.

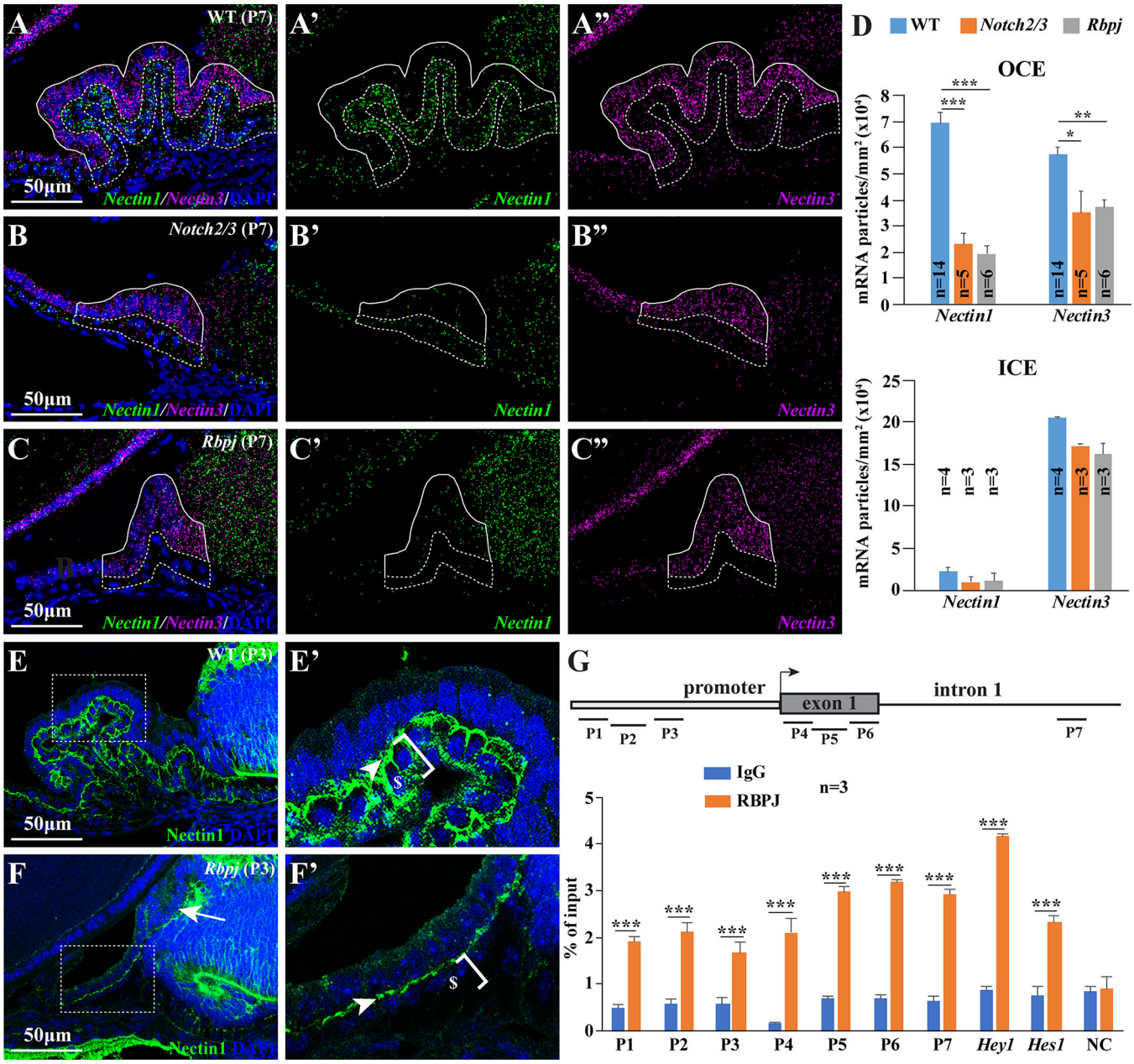

Figure 2. RBPJ regulates *Nectin1* and *Nectin3* expression in the OCE.

Solid and broken lines in **A–C”** highlight the ICE and the OCE of the CB, respectively. (**A-D**) mRNA FISH results show that in the control CB (**A–A”**), *Nectin1* mRNA is primarily expressed in the OCE, whereas Nectin3 is expressed in both the ICE and the OCE but with higher levels in the ICE. *Nectin1* and *Nectin3* are significantly downregulated in the *Notch2/3* double mutant OCE (**B–B”**) and the *Rbpj* mutant OCE (**C–C”**), but *Nectin3* mRNA remain largely unchanged in the mutant ICE. **D**: quantification results. Two-tailed Student’s t-test: *, $P<0.05$; **, $P<0.01$; ***, $P<0.001$. (**E–F**) Nectin1 protein accumulates at the apical and lateral sides of the OCE in the control CB (**E**), but its accumulation is decreased at both the apical and lateral sides of the OCE of the *Rbpj* mutant CB (**F**;

arrow indicates the separated OCE lying on the top of the retina). **E'** and **F'**: highlighted areas in **E** and **F** (broken rectangles) in a high magnification (arrowhead: the apical side; $: OCE; bracket: OCE lateral side). (**G**) ChIP-PCR results show that RBPJ binds to the 7 predicted binding sites in the *Nectin1* regulatory regions (NC: a negative control; *Hey1* and *Hes1*: known NOTCH targets as positive controls). The diagram on the top shows the predicted RBPJ binding sites (#s) in the *Nectin1* gene region. Two-tailed Student's t-test: ***, $P<0.001$. Bars: 50μm.

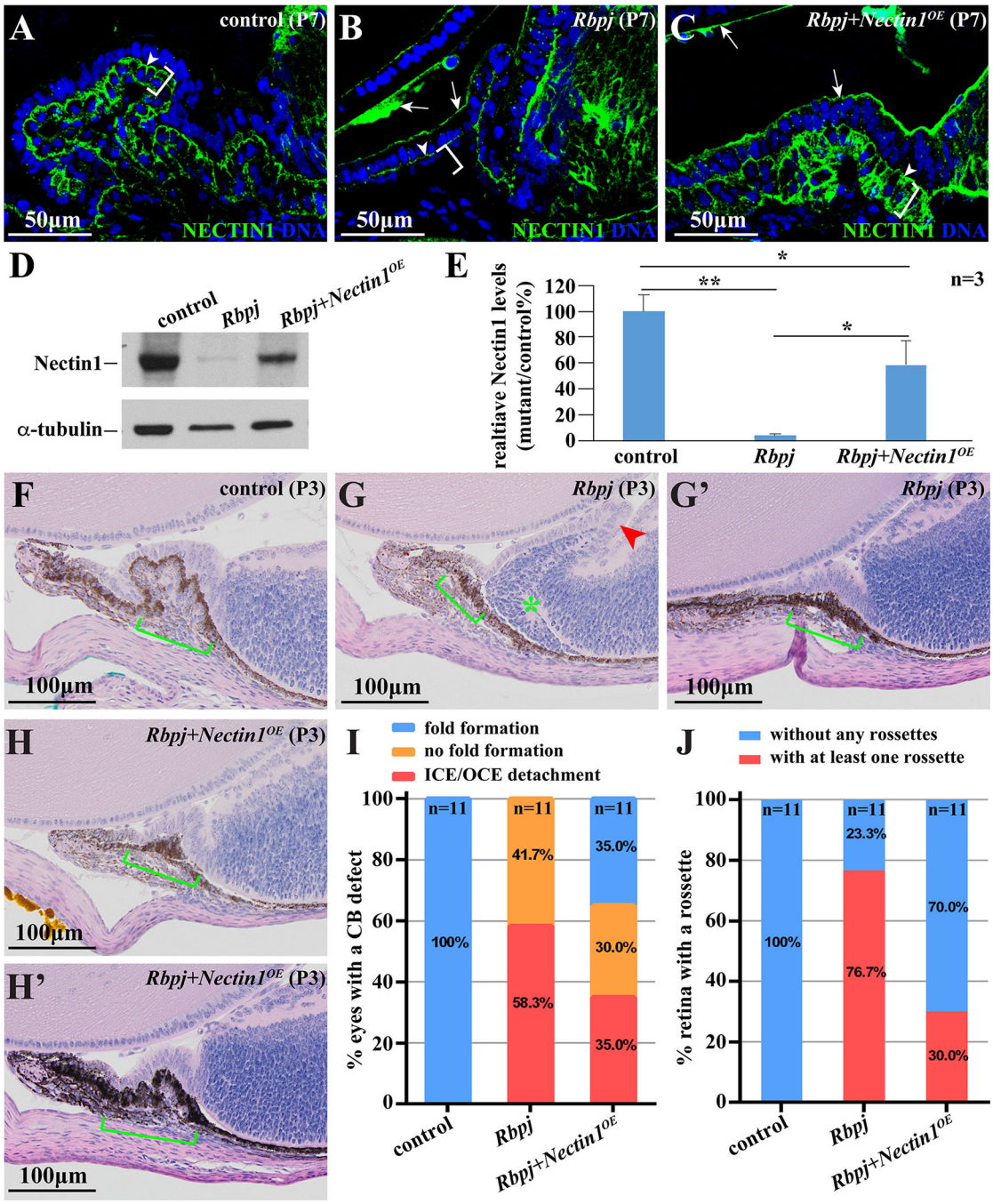

Figure 3. Forced expression of Nectin1 can partially restore ICE-OCE adhesion and morphogenesis of the *Rbpj* mutant CB.

Brackets in **A–C** highlight the lateral side of the OCE, whereas those green ones in **F–H'** indicate CB regions. (**A–C**) Forced *Nectin1* expression (*Nectin1*^{OE}) in the *Rbpj* mutant CB (**C**) can restore the Nectin1 accumulation in the lateral side of the OCE compared to its accumulation in the lateral side of the control CB (**A**) and the *Rbpj* mutant OCE (**B**). Arrowheads indicate the apical side of the OCE (**A–C**), while arrows point to the non-specific highly variable background staining on the surface of the CB and the lens

in the *Rbpj* mutant eyes (**B**, **C**). (**D**, **E**) Western blots showing that Nectin1 protein is significantly downregulated in the Rbpj mutant CBs, and can be significantly restored by Nectin1 overexpression in the CB (internal control: α-tubulin). **E**: quantification results normalized to the controls (three biological replicates). Two-tailed Student's t-test: *, $P<0.05$; **, $P<0.01$. (**F–J**) $Nectin1^{OE}$ in the *Rbpj* mutant CB (**H**, **H'**) can decrease the ICE-OCE detachment, the absence of CB morphogenesis and the rosette formation in the periphery retina caused by *Rbpj* deletion (**G**, **G'**) compared to the control (**F**). Green asterisk (*) marks a retinal rosette. **I** and **J**: quantification results (Note: eye sections with the CB defective on one side and both sides are quantified as 0.5 and 1.0, respectively). Bars: 50μm (**A–C**) and 100μm (**F–H'**).

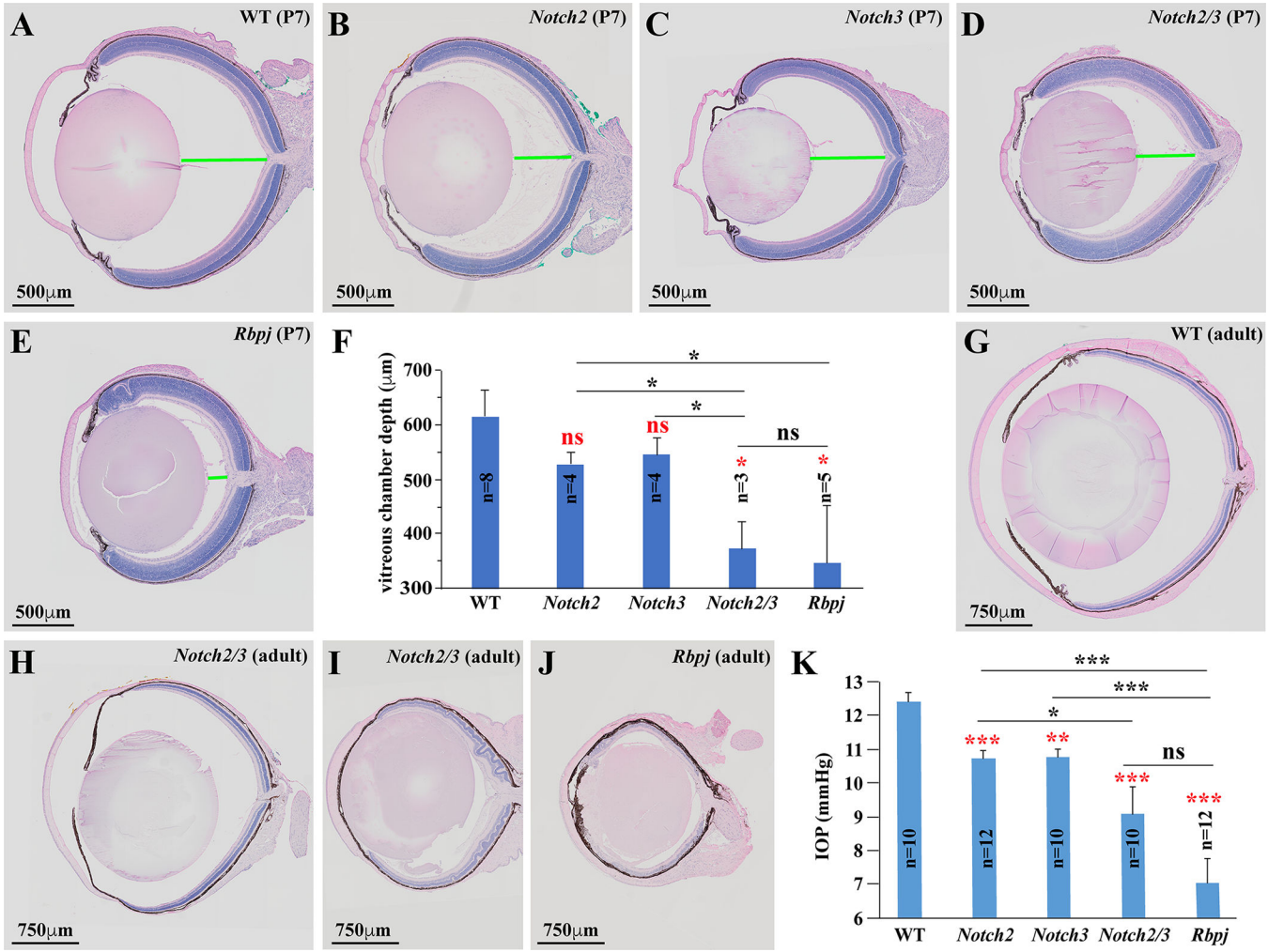

Figure 4. NOTCH2 and NOTCH3 function redundantly via RBPJ to control the formation and maintenance of the vitreous body and maintain adult eye structures.

Green lines indicate the depth of the vitreous body in P7 eyes. In **F** and **K**, red and black asterisks show control-vs-mutant and mutant-vs-mutant comparisons, respectively. (**A–F**) *Notch2/3* (**D**) and *Rbpj* (**E**) mutant P7 eyes exhibit a significant shrinkage of the vitreous, but *Notch2* (**B**) and *Notch3* (**C**) mutant P7 eyes only slightly decrease the depth of the vitreous, compared to the control P7 eye (**A**). **F**: quantification results (red: comparing the mutants with wild-type; black: comparing between the mutants). Two-tailed Student's t-test: *, $P<0.05$; ns, no significance. (**G–J**) *Notch2/3* mutant adult eyes (**H**, **I**) are either smaller than the control adult eye (**G**) or completely degenerate (**I**), while the *Rbpj* mutant adult eye degenerates (**J**). (**K**) Quantification results show that *Notch2/3* and *Rbpj* mutant adult eyes exhibit significantly lower IOP than the control, but *Notch2* and *Notch3* mutant adult eyes exhibit slightly lower IOP (red: comparing the mutants with wild-type; black: comparing between the mutants). Two-tailed Student's t-test: *, $P<0.05$; **, $P<0.01$; ***, $P<0.001$. Bars: 500μm (**A–E**) and 750μm (**G–J**).

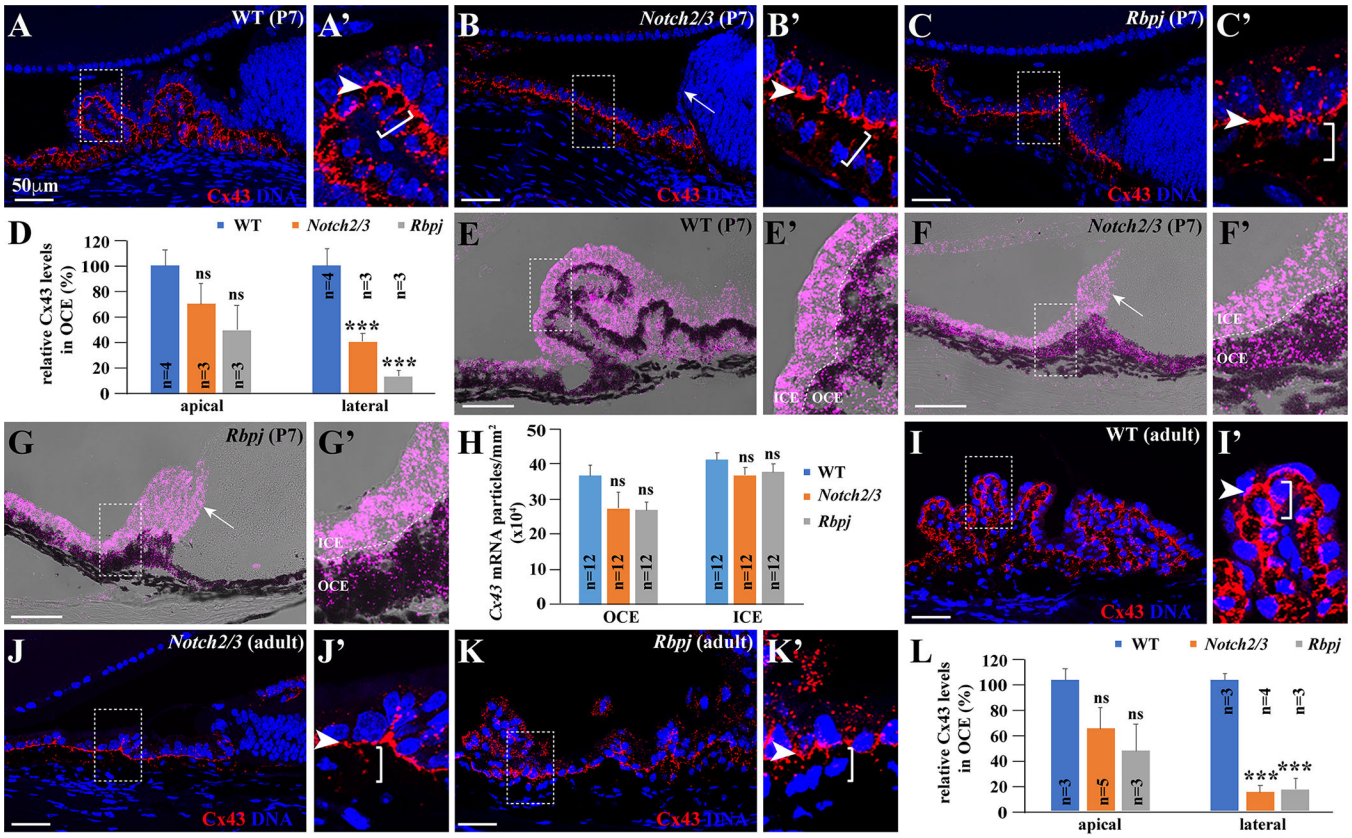

Figure 5. NOTCH2/3-RBPJ signaling is required for maintaining Cx43 protein accumulation in the OCE.

Broken rectangles in **A–C**, **E–G** and **I–K** highlight the CB areas shown in **A'–C'**, **E'–G'** and **I'–K'** at a higher magnification, respectively. Arrowheads and brackets indicate the apical and lateral sides of the OCE, respectively. Arrows in **B**, **F** and **G** point to the separated ICE lying on the top of the retina. (**A–D**) In the P7 control CB (**A**), Cx43 protein accumulates on the cytoplasmic membrane at the apical and lateral sides of the OCE, but its accumulation at the lateral sides of the OCE of the *Notch2/3* (**B**) and *Rbpj* (**C**) mutant CBs is significantly reduced compared to the control. **D**: quantification results on Cx43 protein levels based on fluorescence intensities/area. Two-tailed Student's t-test: ***, $P<0.001$; ns, no significance. (**E–H**) mRNA FISH results show that *Cx43* mRNA expression levels remain similar in both the ICE and OCE of the *Notch2/3* (**F**) and *Rbpj* (**G**) mutant CBs compared to the control (**E**). **H**: quantification results on *Cx43* mRNA levels. Two-tailed Student's t-test: ns, no significance. (**I–L**) Cx43 protein in the adult control CB (**I**) shows expression patterns to that in the P7 CB, but its accumulation at the lateral side of the OCE of the *Notch2/3* (**J**) and *Rbpj* (**K**) mutant adult CBs is significantly reduced. **L**: quantification results on Cx43 in the adult OCE. Two-tailed Student's t-test: ***, $P<0.001$; ns, no significance. Bars: 50μm.

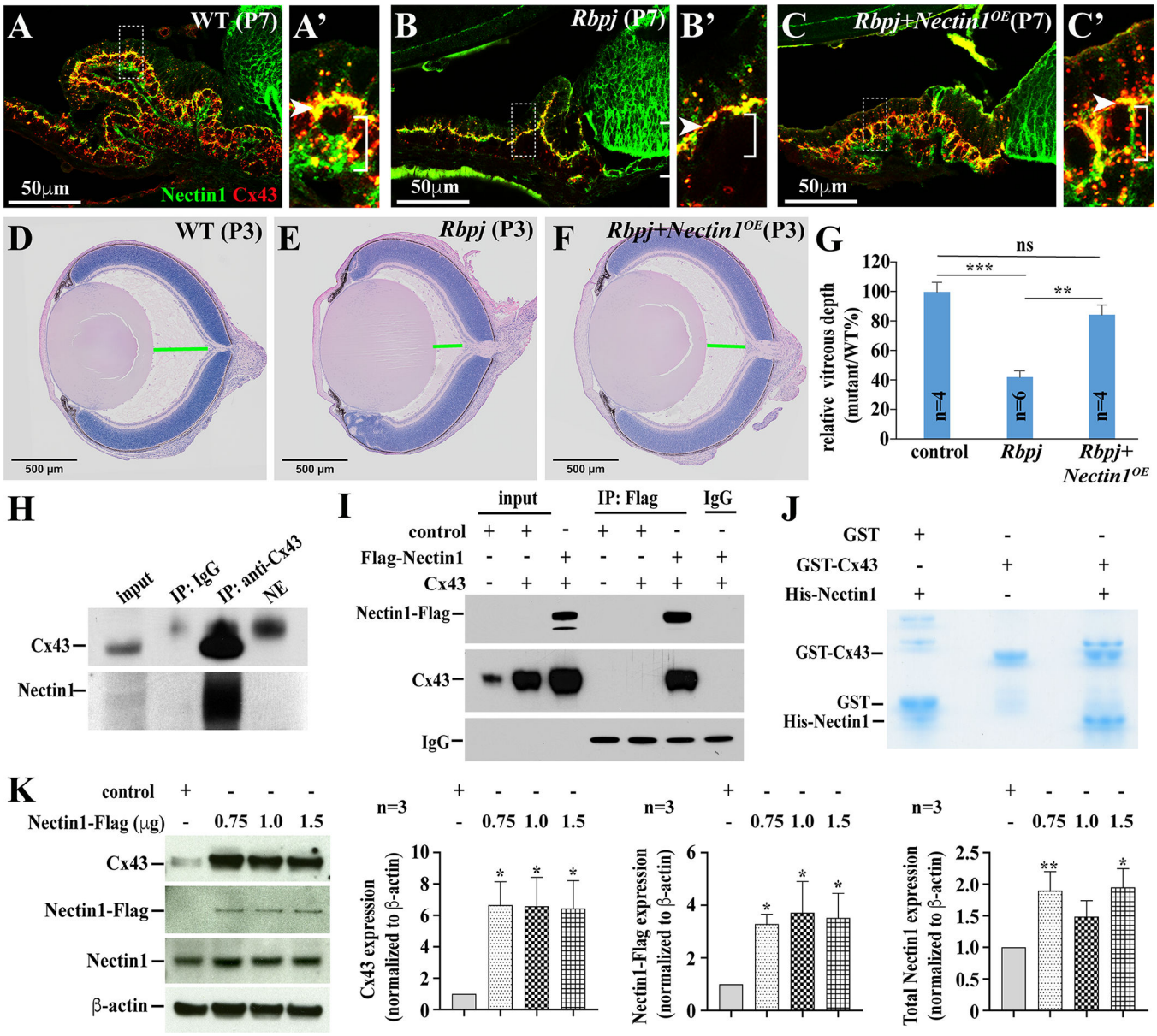

Figure 6. Nectin1 stabilizes and localizes Cx43 protein in the OCE by direct interaction. Brackets indicate the lateral side of the OCE.

(**A–C**) Cx43 and Nectin1 proteins are colocalized at the apical and lateral sides of the OCE in the control CB (**A**), and such colocalization at the lateral side of the OCE of the *Rbpj* (**B**) mutant CB is drastically reduced, but can be restored by *Nectin1*^{OE} (**C**) (**A'–C'**: the highlighted areas by broken rectangles in **A–C** at a higher magnification). (**D-G**) *Nectin1*^{OE} (**F**) can significantly and drastically rescue the vitreous body in the *Rbpj* mutant eye (**E**) compared to the wild-type (**D**) (**G**: quantification results on the depth of the vitreous body of P3-P7 eyes). Two-tailed Student's t-test: **, $P<0.01$; ***, $P<0.001$; ns, no significance. Green lines highlight the vitreous depth. (**H**) Cx43 can pull down Nectin1 protein in the cell extracts of the isolated CBs. (**I**) Flag-tagged Nectin1 can bring down Cx43 in human 293 cell extracts (IgG pulldown as a negative control). (**J**) Purified bacterially expressed GST-

Cx43 C-terminal cytoplasmic domain, but not GST alone, can bring down the purified His-Nectin1 intracellular domain *in vitro*. (**K**) Nectin1 overexpression can stabilize endogenous Cx43 protein in human 293 cells. Two-tailed Student's t-test: *, $P<0.05$; **, $P<0.01$. Bars: 50μm (**A–C**) and 500μm (**D–F**).

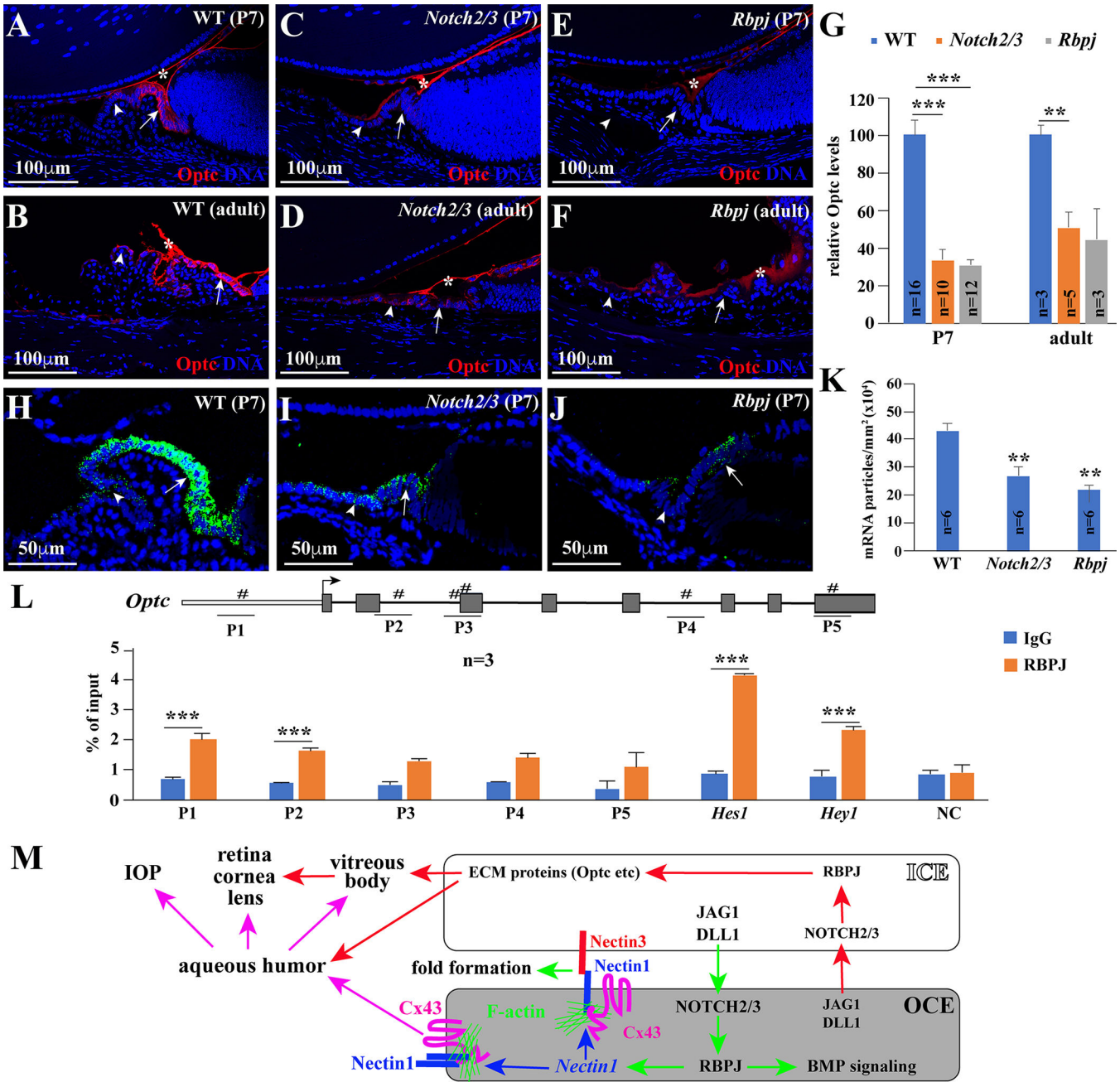

Figure 7. NOTCH-RBPJ signaling directly regulates the expression of vitreous protein Optc.

(**A–G**) Optc is expressed in the posterior ICE of P7 and adult WT CBs (**A**, **B**) and secreted to the vitreous to be deposited on the top of the CB and retina, and its expression is drastically and significantly reduced in *Notch2/3* (**C**, **D**) and *Rbpj* (**E**, **F**) mutant P7 and adult CBs. **G**: quantification results. Two-tailed Student's t-test: **, $P<0.01$; ***, $P<0.001$. (**H–K**) mRNA FISH results show that Optc mRNA is expressed in the posterior ICE of the control P7 CB (**H**), but it is also significantly reduced in *Notch2/3* (**I**) and *Rbpj* (**J**) mutant adult CBs (**K**: quantification results). Two-tailed Student's t-test: **, $P<0.01$. (**L**) ChIP-PCR results show that RBPJ can occupy two out the five predicted sites in the *Optc* gene region

(*Hey1* and *Hes1*: positive controls; NC: negative control). The diagram on the top show the predicted RBPJ binding sites (#s) in the *Optc* gene regions. Two-tailed Student's t-test: ***, $P<0.001$. (**M**) A working model explaining how NOTCH-RBPJ signaling controls ICE-OCE adhesion, CB morphogenesis and secretion. NOTCH2/3-RBPJ signaling in the OCE controls the expression of Nectin1, which works with Nectin3 in the ICE to mediate ICE-OCE adhesion for driving CB morphogenesis. Nectin1 can localized and stabilize Cx43 at the lateral side of the OCE to regulate the aqueous humor secretion, thereby maintaining the vitreous and the IOP. In addition, NOTCH2/3-RBPJ signaling in the ICE controls the expression of the genes encoding vitreous proteins, which are also important for supporting the development and maintenance of cornea, lens and retina. Bars: 100μm (**A–F**) and 50μm (**H–J**).

KEY RESOURCES TABLE

REAGENT or RESOURCE	SOURCE	IDENTIFIER
Antibodies		
Rabbit polyclonal anti-Nectin 1	Santa Cruz Biotechnology	Cat#sc-28639; RRID: AB_2174034
Rabbit polyclonal anti-RBPJK	Abcam	Cat#ab25949; RRID: AB_778155
Rabbit polyclonal anti-Cx43	Cell Signaling Technology	Cat#3512; RRID: AB_2294590
Mouse monoclonal anti-Cx43 (clone 3D8A5)	Thermo Fisher Scientific	Cat#35–5000; RRID: AB_2533207
Goat polyclonal anti-OPTC	R&D system	Cat#AF3547; RRID: AB_2156531
Mouse monoclonal Anti-Rhodopsin (clone Rho 1D4)	EMD Millipore	Cat#MAB5356, RRID:AB_2178961
Goat Polyclonal Anti-Calretinin	Chemicon	Cat#AB1550, RRID:AB_90764
Goat Polyclonal Anti-Collagen type IV	SouthernBiotech	Cat#1340–01 RRID:AB_2721907
Rabbit monoclonal Anti- Vimentin (clone EPR3776)	Abcam	Cat#ab 92547 RRID:AB_10562134
Mouse monoclonal anti-FLAG (clone M2)	SIGMA-ALDRICH INC	Cat#F3165; RRID: AB_259529
Mouse monoclonal anti-β-actin (clone AC-15)	Abcam	Cat#ab49900; RRID: AB_867494
Mouse monoclonal anti-α-Tubulin (clone DM1A)	Sigma-Aldrich	Cat# T9026; RRID: AB_477593
Chicken polyclonal anti-GFP	Invitrogen	Cat#A10262; RRID: AB_2534023
Rabbit polyclonal anti-Nectin3	Santa Cruz Biotechnology	Cat#sc-28637; RRID: AB_2284699
Donkey anti-rabbit Alexa Fluor 488-conjugate	Invitrogen	Cat#A21206; RRID: AB_ 2535792
Donkey anti-rabbit Alexa Fluor 568-conjugate	Invitrogen	Cat#A10042; RRID: AB_2534017
Donkey anti-goat Alexa Fluor 488-conjugate	Invitrogen	Cat#A11055; RRID: AB_2534102
Donkey anti-goat Alexa Fluor 568-conjugate	Invitrogen	Cat#A11057; RRID: AB_2534104
Donkey anti-mouse Alexa Fluor 568-conjugate	Invitrogen	Cat#A10037; RRID: AB_2534013
Donkey anti-mouse Alexa Fluor 647-conjugate	Invitrogen	Cat#A31571; RRID: AB_162542
Bacterial and Virus Strains		
N/A		
Biological Samples		
N/A		
Chemicals, Peptides, and Recombinant Proteins		
GoTaq G2 Green Master Mix	Promega Corporation	Cat#M7823
Hartman's Fixative	SIGMA-ALDRICH INC	Cat#H0290
4% paraformaldehyde in 1xPBS	Thermo Fisher Scientific	Cat#J19943-K2
POWER BLOCK 10X	BIOGENEX LABORATORIES	Cat#HK085–5K
4',6-diamidino-2-phenylindole (DAPI)	Sigma-Aldrich	Cat#D9542
5-ethynyl-2-deoxyuridine (EdU)	TCI	Cat#E1057
Vectashield Mounting Medium for Fluorescence	Vector Laboratories	Cat#H-1000
ProLong™ Glass Antifade Mountant	THERMO FISHER SCIENTIFIC	Cat#P36982
DMEM, high glucose, pyruvate	ThermoFisher Scientific	Cat#11995065
FBS	ThermoFisher Scientific	Cat#16000044
Protein A/G PLUS-Agarose	Santa Cruz	Cat#sc-2003

REAGENT or RESOURCE	SOURCE	IDENTIFIER
Mouse Negative Control Primer Set 1	Active Motif: Enabling Epigenetics Research	Cat#71011
Pierce™ Glutathione Agarose	ThermoFisher Scientific	Cat#16102BID
HisPur™ Ni-NTA Superflow Agarose	ThermoFisher Scientific	Cat#25217
Critical Commercial Assays		
Rabbit-on-Rodent HRP-Polymer	BioCare Medical	Cat#RMR622L
TSA-plus Fluorescein system	PerkinElmer	Cat#NEL741001KT
Click-iT™ EdU Alexa Fluor™ 488 Imaging Kit	Thermo Fisher Scientific	Cat#C10337
Pierce™ Agarose ChIP Kit	Thermo Fisher Scientific	Cat#26156
Mem-PER™ Plus Membrane Protein Extraction Kit	Thermo Fisher Scientific	Cat#89842
Deposited Data		
N/A		
Experimental Models: Cell Lines		
Human: 293T Cell lines	ATCC	Cat#CRL-1573
Experimental Models: Organisms/Strains		
Mouse: *C57BL/6J*	LASF of Stowers Institute for Medical Research	JAX: 000664
Mouse: *CD-1*	LASF of Stowers Institute for Medical Research	JAX: 003814
Mouse: *Z/EG*	LASF of Stowers Institute for Medical Research	JAX: 003920
Mouse: *Tyrp1-Cre*	Mori et al., 2002	MGI: 2387296
Mouse: *Tyrp2-Cre*	Davis et al., 2009	MGI: 4358082
Mouse: $Notch2^{fx/fx}$	McCright et al., 2006	MGI: 3617328
Mouse: $Notch3^{-/-}$	Krebs et al., 2003	MGI: 2687010
Mouse: $Rbpj^{fx/fx}$	Tanigaki et al., 2002	MGI: 3583755
Mouse: *CBA/CaJ*	LASF of Stowers Institute for Medical Research	JAX: 000654
Mouse: *C57BL/10J*	LASF of Stowers Institute for Medical Research	JAX: 000665
Mouse: *CAG>STOP>Nectin1-Flag*	This paper	See STAR Methods
Oligonucleotides		
See Table S1 for the primers for genotyping	Integrated DNA Technologies, Inc.	N/A
See Table S2 for the primers for ChIP-qPCR	Integrated DNA Technologies, Inc.	N/A
See Table S3 for the probe sets for RNA in situ Hybridization	Thermo Fisher Scientific	N/A
Recombinant DNA		
pCMV6-Myc-Nectin1	Origene	Cat#RC215930
pCMV6XL4	Origene	Cat#PCMV6XL4
pGEX-4T1/CX43-C-terminal (257–382)	This study	See STAR Methods
pET28a/Nectin 1-C-terminal (313–515)	This study	See STAR Methods
Software and Algorithms		

REAGENT or RESOURCE	SOURCE	IDENTIFIER
Fiji-win64	Schindelin, et al., 2012. Schneider et al., 2012	https://imagej.nih.gov/ij/ https://imagej.net/Fiji
GraphPad Prism 8 for Windows 64-bit	GraphPad Software	www.graphpad.com
Real-Time Analysis (RTA) version 1.17.20.0	Illumina	https://www.illumina.com/
Other		